

Superconductivity of LaH_{10} and LaH_{16} polyhydrides

Ivan A. Kruglov,^{1,2,} Dmitrii V. Semenok,^{1,3,*} Hao Song,⁹ Radosław Szczęśniak,^{4,5} Izabela A. Wrona,⁴ Ryosuke Akashi,⁶ M. Mahdi Davari Esfahani,⁷ Defang Duan,⁹ Tian Cui,⁹ Alexander G. Kvashnin,^{3,1} and Artem R. Oganov^{3,2,8,*}*

¹ Moscow Institute of Physics and Technology, 9 Institutsky Lane, Dolgoprudny 141700, Russia

² Dukhov Research Institute of Automatics (VNIIA), Moscow 127055, Russia

³ Skolkovo Institute of Science and Technology, Skolkovo Innovation Center, 3 Nobel Street, Moscow 121205, Russia

⁴ Institute of Physics, Jan Dlugosz University in Częstochowa, Ave. Armii Krajowej 13/15, 42-200 Częstochowa, Poland

⁵ Institute of Physics, Częstochowa University of Technology, Ave. Armii Krajowej 19, 42-200 Częstochowa, Poland

⁶ University of Tokyo, 7-3-1 Hongo, Bunkyo, Tokyo 113-8654, Japan

⁷ Department of Geosciences and Center for Materials by Design, Institute for Advanced Computational Science, State University of New York, Stony Brook, NY 11794-2100, USA

⁸ International Center for Materials Discovery, Northwestern Polytechnical University, Xi'an 710072, China

⁹ Key State Laboratory of Superhard Materials, Jilin University, Changchun, China

Corresponding authors

*Ivan A. Kruglov, e-mail: ivan.kruglov@phystech.edu

*Dmitrii V. Semenok, e-mail: dmitrii.semenok@skoltech.ru

*Artem. R. Oganov, e-mail: a.oganov@skoltech.ru

ABSTRACT. Recent experiments have established previously predicted LaH_{10} as the highest-temperature superconductor, with T_C up to 250–260 K [1]. In this work we explore the high-pressure phase stability and superconductivity of lanthanum hydrides LaH_m . We predict the stability of the hitherto unreported polyhydride $P\ 6/mmm$ - LaH_{16} at pressures above 150 GPa; at 200 GPa, its predicted superconducting T_C is 156 K, the critical field $\mu_0 H_C(0)$ is approximately 35 T, and the superconducting gap is up to 35 meV. We revisit the superconductivity of LaH_{10} and find its T_C to be up to 259 K at 170 GPa from solving the Eliashberg equation and 271 K from solving the gap equation in the density functional theory for superconductors (SCDFT), which also allows us to compute the Coulomb pseudopotential μ^* for LaH_{10} and LaH_{16} . The presence of several polymorphic modifications of LaH_{10} may explain the variety in its measured T_C values [1, 2].

Introduction

Recently, superhydrides of various elements attracted a great attention: they were first predicted and then experimentally proven to exhibit a record high-temperature superconductivity under a high pressure. According to the Bardeen–Cooper–Schrieffer (BCS) theory, the metallic hydrogen is expected to be a high- T_C superconductor [3–6], yet the pressure needed for its formation is too high (~ 500 GPa) [7]. Ashcroft proposed to stabilize states similar to metallic hydrogen at lower pressures by creating hydrogen-rich hydrides, where the hydrogen atoms experience an additional “chemical” pressure [8]. Following this, many theoretical predictions of remarkable high-temperature superconductors (HTSC) were made, e.g., in the Ca-H [9], Y-H [10], H-S [11], Th-H [12], Ac-H [13], and La-H [10] systems. In all these systems, the high- T_C superconductors have unusual chemical compositions, like H_3S , LaH_{10} , or CaH_6 . The formation of such compounds, violating the rules of classical chemistry, commonly takes place under pressure [15].

The first experimental proof was obtained for H_3S with measured $T_C = 203$ K at 155 GPa [16] (the predicted value was 191–204 K at 200 GPa [11]). The confidence in such predictions has greatly increased because of their agreement with the observations, stimulating a wave of theoretical studies of superconductivity in hydrides [10, 12, 13, 16–29]. The recent theoretical

work on the La-H and Y-H systems [10] under pressure showed that at 300 GPa LaH_{10} and YH_{10} may display room-temperature superconductivity (at 286–326 K). According to that theoretical study, at pressures below 200 GPa LaH_{10} has the $R\bar{3}m$ symmetry, which changes to $Fm\bar{3}m$ at higher pressures. In the experiments by Geballe et al. [20], $R\bar{3}m$ - LaH_{10} was found at ≤ 160 to 170 GPa, while $Fm\bar{3}m$ - LaH_{10} was seen at higher pressures. The experimentally observed sharp drop in resistivity in the LaH_{10} samples was the first evidence of superconductivity in this system [1, 2]. Different studies showed a series of superconducting-like transitions with T_c of 70 and 112 K [1], 210–215 K [1], 244–250 K [1, 2], and 260–280 K [1]. This discrepancy in the T_c values may be caused by the coexistence of lanthanum hydrides having different compositions and crystal structures in the studied samples. To address these questions, we predicted the stable compounds in the La-H system using the variable-composition evolutionary algorithm USPEX [30–32]. While most studies report only T_c and assume $\mu^* = 0.1\text{--}0.15$ for the calculations, here we obtain T_c using various approaches including the superconducting DFT, which requires no assumption of μ^* , and also compute other properties, such as the critical magnetic field [1].

Computational Details

The evolutionary algorithm USPEX [30–32] is a powerful tool for predicting thermodynamically stable compounds of given elements. To predict thermodynamically stable phases in the La-H system, we performed variable-composition crystal structure searches at pressures from 50 to 200 GPa. The first generation of 100 structures was created using a random symmetric [32] and topological structure generators [33] with the number of atoms in the primitive unit cell ranging from 8 to 16, while the subsequent generations contained 20% of random structures, and the rest 80% of structures were created using the heredity, softmutation, and transmutation operators. Here, the evolutionary searches were combined with structure relaxations using the density functional theory (DFT) [34, 35] within the generalized gradient approximation (the Perdew–Burke–Ernzerhof functional) [36], and the projector-augmented wave method [37, 38] as implemented in the VASP package [39–41]. The plane wave kinetic energy cutoff was set to 500 eV and the Brillouin zone was sampled by Γ -centered k -points meshes with a resolution of $2\pi \times 0.05 \text{ \AA}^{-1}$. This methodology was used and proved to be very effective in our previous works (e.g., [12–14]).

The calculations of the critical temperature and electron-phonon coupling (EPC) parameters were carried out using Quantum ESPRESSO (QE) package [42] within the density functional perturbation theory [43], employing the plane-wave pseudopotential method and Perdew–Burke–Ernzerhof exchange-correlation functional [36]. The convergence tests showed that 90 Ry is a suitable kinetic energy cutoff for the plane wave basis set. The electronic band structures and phonon densities of states were calculated using both VASP (the finite displacement method using PHONOPY [44, 45]) and QE (the density functional perturbation theory [43]), which demonstrated a good consistency.

In our calculations of the EPC parameter λ , the first Brillouin zone was sampled using a $4 \times 4 \times 4$ q -points mesh and a denser $16 \times 16 \times 16$ k -points mesh (with the Gaussian smearing and $\sigma = 0.02$ Ry, which approximates the zero-width limits).

For LaH_{10} and LaH_{16} , we also estimated T_c by solving the gap equation within the density functional theory for superconductors (SCDFT) [46, 47]:

$$\Delta_{nk}(T) = -Z_{nk}(T)\Delta_{nk}(T) - \frac{1}{2}\sum K_{nkn'k'}(T) \frac{\tanh\beta E_{n'k'}}{E_{n'k'}} \Delta_{n'k'}(T). \quad (1)$$

Here, $E_{nk} = \sqrt{[\Delta_{nk}(T)]^2 + [\xi_{nk}]^2}$, with ξ_{nk} being the normal-state energy eigenvalue of \hat{H}_e labeled by the band index n and wave vector k measured from the Fermi level. The “order parameter” $\Delta_{nk}(T)$ depends on n and k , not on the frequency ω ; it is defined in a way different from that in the Eliashberg equation and is proportional to the thermal average $\langle c_{nk\uparrow}c_{n-k\downarrow} \rangle$, with $c_{nk\sigma}$ being the annihilation operator of the spin state $nk\sigma$ [46]. The interaction effects treated in the Eliashberg equation are included with the kernels entering this gap equation; $Z_{nk} = Z_{nk}^{ph}$;

$K_{nkn'k'} = K_{nkn'k'}^{ph} + K_{nkn'k'}^{el}$. Here we included the mass-renormalization by the phonon exchange with $Z_{nk}^{ph} = Z^{ph}(\xi_{nk})$ (see Eq. (40) in [48] and an improved form of Eq. (24) in [47] to consider the nonconstant electronic density of states), the phonon-mediated electron-electron attraction with $K_{nkn'k'}^{PH} = K^{PH}(\xi_{nk}, \xi_{n'k'})$ (Eq. (23) in [47]), and the screened Coulomb repulsion $K_{nkn'k'}^{el}$ (Eq. (3) in [53]). Unlike the Eliashberg equation, the SCDFT gap equation does not contain the frequency ω . Nevertheless, the retardation effect [50] is approximately incorporated [47]. The absence of ω enables us to treat all electronic states in a wide energy range of ± 30 eV at an affordable computational cost, and therefore estimate T_C without the empirical Coulomb pseudopotential μ^* . We estimated T_C as the temperature where the nontrivial solution of this gap equation vanishes (see Supporting Information [51]).

The Coulomb pseudopotential μ^* , included in the Eliashberg equation and its approximate solutions such as the Allen–Dynes (A–D) equation, quantifies the impact of the renormalized Coulomb repulsion. Its value can in principle be estimated with the matrix element of the screened Coulomb interaction and energy scales of the electrons and phonons [50, 51], but practically it is determined by fitting the calculated observables with the experimental data or simply by accepting the typical values (e.g., ~ 0.10 – 0.13) from such previous fitting results [53]. On the other hand, while the SCDFT gives us the framework free from empirical parameters such as μ^* , deriving from it some interesting observables is difficult compared with the Eliashberg theory. Especially, the spectral gap at absolute zero, being defined within the Green’s function framework, is not directly accessible within the SCDFT. To estimate several observable quantities, we took a hybrid approach reconciling these frameworks: Determining the value of μ^* so that the Eliashberg (or Allen–Dynes) equation reproduces T_C derived from the SCDFT gap equation [54] and then employing it in later calculations within the Eliashberg theory. In this approach, we presume that the retardation effect [50] can be expressed by a single parameter, μ^* ; possible drawbacks of this method are discussed later.

In this work we did not consider the effect of anharmonicity on the dynamic and superconducting properties of lanthanum hydrides. While this effect can be important, previous studies showed that the superconducting properties predicted within the “conventional” approach are in relatively good agreement with the experimental data.

Results and Discussion

I. Stability of La–H phases

We performed the variable-composition evolutionary searches for stable compounds and crystal structures at 50, 100, 150, and 200 GPa. The thermodynamic convex hulls are shown in Fig. 1. By composition, stable phases are those that appear on the convex hull. Thus, at 50 GPa we found $Fm\bar{3}m$ -LaH, $Pnma$ -LaH₃, $Cmc2_1$ -LaH₇, and Cc -LaH₉ to be stable (Fig. 1a). At 100 GPa, LaH₇ and LaH₉ disappear from the convex hull, while four new hydrides become stable: Cm -LaH₂, $Cmcm$ -LaH₃, $P\bar{1}$ -LaH₅, and $P\bar{4}/nmm$ -LaH₁₁ (Fig. 1b). At 150 GPa, the chemistry of lanthanum hydrides is much richer: $P\bar{6}/mmm$ -LaH₂, $Cmcm$ -LaH₃, $I\bar{4}/mmm$ -LaH₄, $P\bar{1}$ -LaH₅, $Fm\bar{3}m$ -LaH₁₀, and $P\bar{6}/mmm$ -LaH₁₆ phases become stable (Fig. 1c). At 200 GPa, only five stable lanthanum hydrides remain on the convex hull: $P\bar{6}/mmm$ -LaH₂, $Cmmm$ -La₃H₁₀, $I\bar{4}/mmm$ -LaH₄, $Fm\bar{3}m$ -LaH₁₀, and $P\bar{6}/mmm$ -LaH₁₆. Our results are similar to those from [55], the main difference being that we predict the new LaH, La₃H₁₀, and LaH₁₆ compounds and also find that LaH₁₀ is stable at pressures above 135 GPa, which is consistent with the experimental data [1, 2]. Yet, we found $Fm\bar{3}m$ -LaH₁₀ to be more stable than $R\bar{3}m$ -LaH₁₀ at pressures above 150 GPa. The $R\bar{3}m \rightarrow Fm\bar{3}m$ phase transition occurs at 128 GPa (Supporting Information Fig. S19 [51]). Taking into account the zero-point energy correction, the pressure of this phase transition shifts to 135 GPa, which is consistent with the experimental phase transition pressure of 160 GPa [20]. Below we discuss the superconducting properties of the previously known lanthanum hydrides

and explore the crystal structure and SC properties of the newly found LaH_{16} . The crystal structure data are summarized in Supporting Information Table S1 [51].

Stoichiometry 1:1 is common for various hydrides (e.g., U-H [14], Fe-H [23], and many others [56]). $Fm\bar{3}m$ - LaH has a structure of a rock salt type, with La–H distance of 2.26 Å at 50 GPa. In the $Pnma$ - LaH_3 structure, the La atoms have a 10-fold coordination and H–H distances are too long to be considered bonding (2.28 Å at 50 GPa). In $Cmc2_1$ - LaH_7 , the lanthanum atoms have a 13-fold coordination, while the shortest H–H distances (0.81 Å at 50 GPa) are clearly bonding and quite close to the H–H bond length in the molecular hydrogen (0.74 Å).

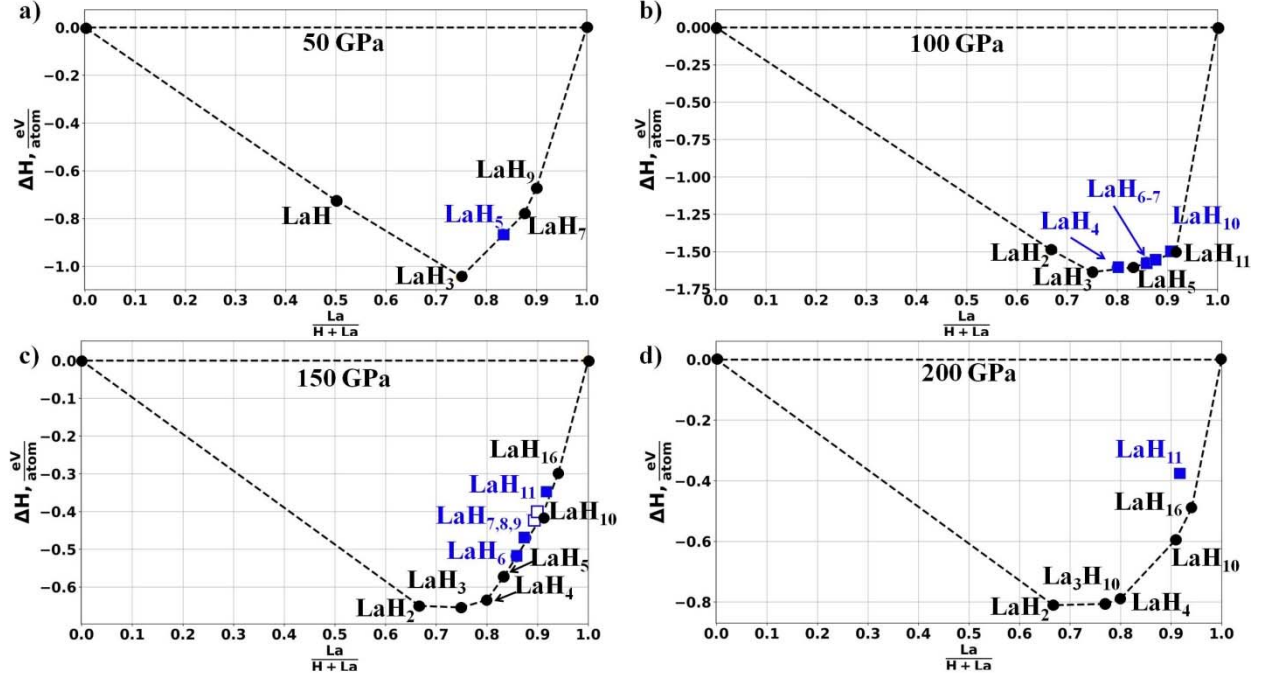


Fig. 1. Convex hull diagrams for the La-H system at a) 50, b) 100, c) 150, and d) 200 GPa. The metastable and stable phases are marked by blue squares and black circles, respectively.

Our results at 150 GPa are consistent with those in [10]: $P6/mmm$ - LaH_2 , $Cmcm$ - LaH_3 , $Immm$ - LaH_4 , and $P\bar{1}$ - LaH_5 phases are thermodynamically stable. Previous studies explored only simple fixed stoichiometries, whereas the USPEX method used here can automatically detect even nontrivial stoichiometries, which helped us find a new phase, $Cmmm$ - La_3H_{10} , at 200 GPa. This phase is structurally related to $Cmcm$ - LaH_3 , has an additional hydrogen atom in the tripled unit cell, and its lattice parameter c is 3 times larger.

Superconducting properties for the most promising LaH_{10} and LaH_{16} phases were calculated using the SCDFT method, then the μ^* value was determined by adjusting T_C obtained through the numerical solution of the Eliashberg equation to that from the SCDFT. For comparison, the μ^* values determined using the A-D formula are presented in Supporting Information Table S2 [51]. We find a significant difference in the μ^* values obtained, depending on whether the Eliashberg or A-D equation were used, because the LaH_x systems are classified as the strong-coupling case where these equations give substantially different values of T_C [1].

II. Superconductivity of LaH_{10} phases

Superconductivity of LaH_{10} has been confirmed in experiments [1, 2]. Our analysis is based on the T_C calculation using the SCDFT, Eliashberg function $\alpha^2 F(\omega)$, and the electronic density of states for $R\bar{3}m$ - and $Fm\bar{3}m$ - LaH_{10} phases. The experimental observations found the maximum $T_C \sim 251$ K at 168 GPa [2] or $T_C \sim 260$ K at 180 GPa [1], which is close to the $R\bar{3}m$ - $Fm\bar{3}m$ phase transition (but in the cubic phase). The value of the Coulomb pseudopotential μ^* for the LaH_{10} phases determined using the SCDFT equals 0.2 at 200 GPa (see Supporting Information [51]).

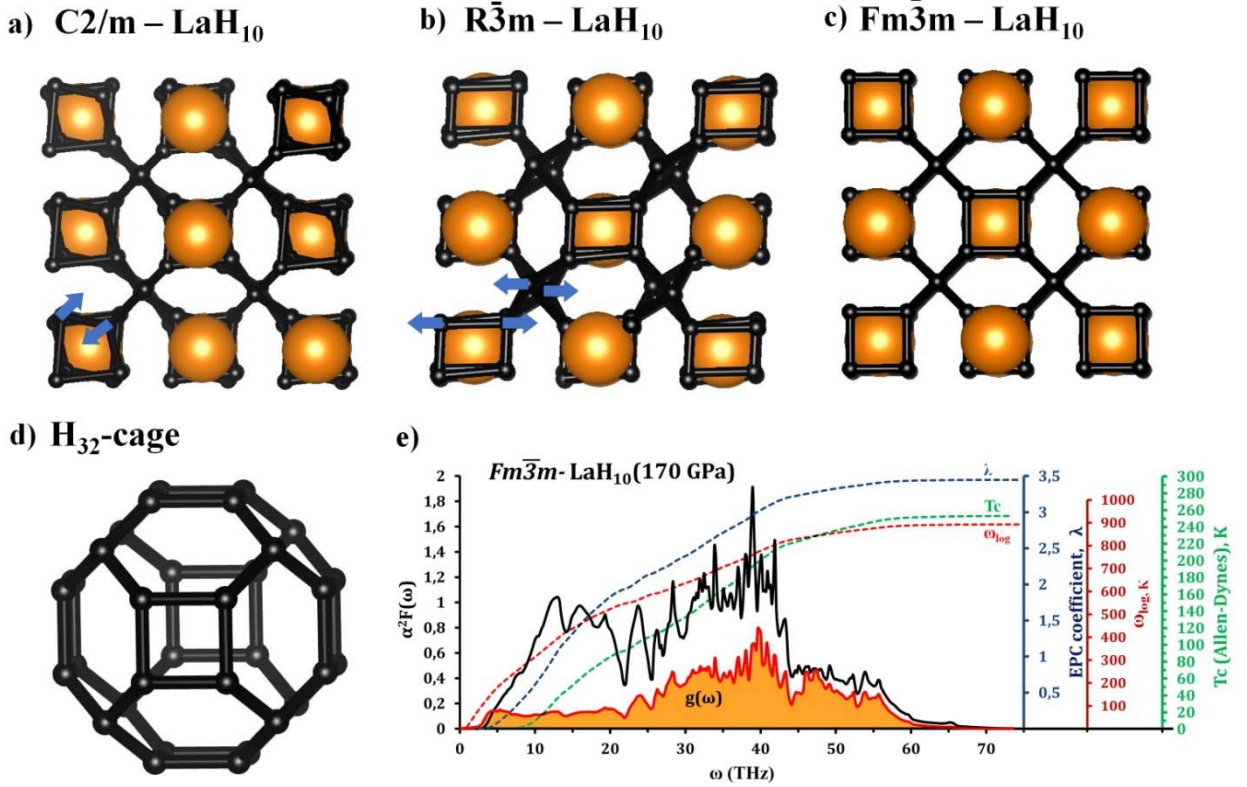


Fig. 2. Crystal structures of a) $C\bar{2}/m$ -LaH₁₀, b) $R\bar{3}m$ -LaH₁₀, c) $Fm\bar{3}m$ -LaH₁₀, and d) hydrogen H₃₂ cage common for these phases; e) the Eliashberg $\alpha^2 F(\omega)$ function (black curve), phonon density of states (orange), cumulative ω_{\log} (red), EPC coefficient λ (blue), and critical transition temperature T_c (green) of $Fm\bar{3}m$ -LaH₁₀ at 170 GPa. The crystal structures were generated using VESTA software [57]; the atoms of La and hydrogen are shown as large orange and small black balls, respectively; blue arrows show displacements of the hydrogen atoms in comparison with the cubic H₈ cluster.

For $Fm\bar{3}m$ -LaH₁₀, the calculations within the DFPT give a very high EPC coefficient $\lambda = 3.75$, which leads to $T_c = 271$ K at 200 GPa (see Table 1 and Supporting Information for details [51]). At 200 and 250 GPa, the calculated volumes (30.4 and 28.5 Å³, respectively) and the electronic density of states, $N(E_F) = N(0) = 10.6$ and 10.0 states/f.u./Ry, allowed us to estimate the Sommerfeld constant (Table 1) at 0.016 and 0.011 J/mol·K², which is very close to that of $Fm\bar{3}m$ -ThH₁₀ (0.011 J/mol·K² [12]) at 100 GPa. These constants were used to calculate the critical magnetic field ($\mu_0 H_c(0)$) and the jump in specific heat $\Delta C/T_c$ (Table 1). The calculation details are presented in Supporting Information [51].

The Eliashberg function for the cubic $Fm\bar{3}m$ -LaH₁₀ at 200 GPa is shown in Fig. 2e (for other pressure values and phases, see Supporting Information [51]). The numerical solution of the Eliashberg equation for the cubic LaH₁₀ at the experimental pressure of 170 GPa results in $T_c = 259$ K (Table 1), which is in close agreement with the theoretical results [10] and experiments [1, 2].

The calculated critical temperature for $R\bar{3}m$ -LaH₁₀ at 150 GPa is 203 K (Table 1), much lower than that of the $Fm\bar{3}m$ modification, which can explain the experimental results of Drozdov et al. [1].

Table 1. Parameters of the superconducting state of $Fm\bar{3}m$ -LaH₁₀ and $R\bar{3}m$ -LaH₁₀ from the Eliashberg equation (with $\mu^* = 0.2$).

Parameter	$Fm\bar{3}m$ -LaH ₁₀				$R\bar{3}m$ -LaH ₁₀	
	170 GPa	200 GPa	210 GPa	250 GPa	150 GPa	165 GPa
N_f , states/f.u./Ry	11.2	10.6	10.3	10.0	12.2	11.0
λ	3.94	3.75	3.42	2.29	2.77	2.63
ω_{log} , K	801	906	851	1253	833	840
T_C , K	259	271*	249	246	203	197
$\Delta(0)$, meV	62.0	63.7	59.6	48.0	48.5	43.7
$\mu_0 H_C(0)$, T**	89.0	95.0	81.0	66.7	72.7	71.0
$\Delta C/T_C$, mJ/mol·K ²	31.5	44.7	34.5	33.4	42.8	25.7
γ , J/mol·K ²	0.019	0.016	0.015	0.011	0.018	0.018
$R_\Delta = 2\Delta(0)/k_B T_C$	5.54	5.46	5.55	5.00	5.55	5.54

* SCDF (see Supporting Information [51])

** The experimentally measured critical magnetic field is 95–136 T [1]

The isotope coefficient β was calculated using the A-D formula (see Supporting Information [51]). With $\mu^* = 0.11$ used for the A-D equation, the calculated value was the same, $\beta = 0.48$, for both $Fm\bar{3}m$ -LaH₁₀ and $R\bar{3}m$ -LaH₁₀ at 200 GPa. Using the isotope coefficient β , the critical temperature of lanthanum decadeuteride can be determined as $T_D = 2^{-\beta} \cdot T_H$, resulting in 181 K for $Fm\bar{3}m$ -LaD₁₀ and 154 K for $R\bar{3}m$ -LaD₁₀. The experimentally measured T_C for $Fm\bar{3}m$ -LaD₁₀ is 168 K [1], corresponding with our prediction.

III. Prediction of high- T_C LaH₁₆

Perhaps the most intriguing finding of our work is the prediction of the thermodynamic stability of $P6/mmm$ -LaH₁₆ at pressures above 150 GPa (Fig. 1c). This phase has a crystal structure different from the previously predicted AcH_{16} [13]. The lanthanum atoms form an *hcp* sublattice and are coordinated by 12 hydrogen atoms (Fig. 3a). These H-units consist of three parallel layers of hydrogen atoms. The distances between the hydrogen atoms in the first, second, and third layers at 150 GPa are 1.07, 1.02, and 1.07 Å, respectively. The distance between the closest hydrogen atoms from different layers is 1.25 Å, so these layers form infinite 2D networks. The crystal structures of all predicted phases are summarized in Supporting Information Table S1 [51].

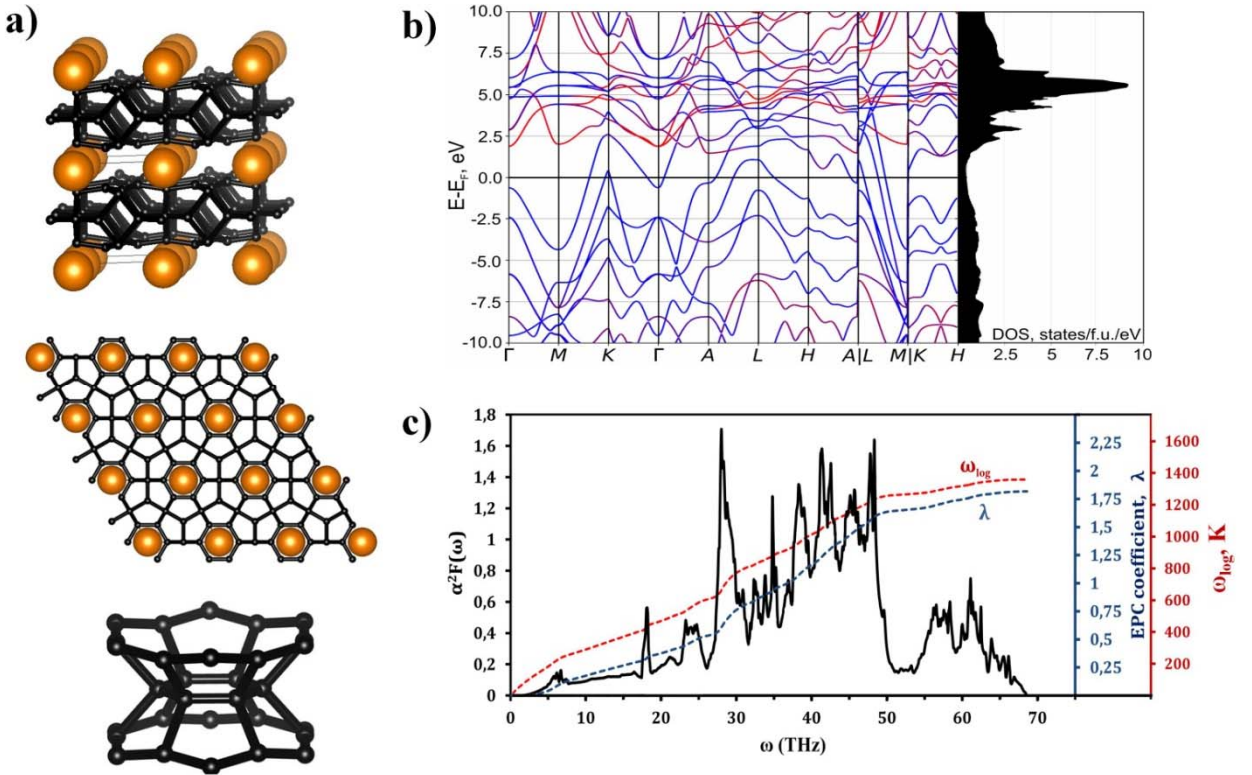


Fig. 3. a) Crystal structure of $P\ 6/mmm$ -LaH₁₆ at 150 GPa; b) band structure and DOS of LaH₁₆ (red lines are for La, blue — for H) at 250 GPa; c) the Eliashberg function $\alpha^2 F(\omega)$ (black), cumulative ω_{log} (red), and the EPC coefficient λ (blue) of $P6/mmm$ -LaH₁₆ at 200 GPa.

$P\ 6/mmm$ -LaH₁₆ shows very little dependence of the electronic density of states on the pressure at 200–300 GPa. The Eliashberg function of $P\ 6/mmm$ -LaH₁₆ computed at 200 GPa is shown in Fig. 3c (for other pressure values, see Supporting Information [51]). The EPC coefficient of LaH₁₆ (Table 2) is approximately two times lower than that of LaH₁₀. The SCDFT calculations for LaH₁₆ at 200 GPa yield $T_C = 156$ K, which leads to the calculated $\mu^* = 0.41$, an anomalously large value compared to the commonly accepted 0.1–0.15 interval. This abnormal value of μ^* for LaH₁₆ is caused by the complex behavior of DOS(E) in the vicinity of $E_F \pm 1$ eV (see Supporting Information [51]). We used $\mu^* = 0.41$ in the numerical solution of the Eliashberg equation to calculate the superconducting properties of $P\ 6/mmm$ -LaH₁₆ (Table 2). T_C of this phase shows a weak pressure dependence ($dT_C/dP = -0.3$ K/GPa).

Table 2. Parameters of the superconducting state of $P\ 6/mmm$ -LaH₁₆ at 200–300 GPa calculated using the Eliashberg equation with $\mu^* = 0.41$. Here γ is the Sommerfeld constant calculated using Eq. *Ошибка! Источник ссылки не найден..*

Parameter	200 GPa	250 GPa	300 GPa
N_f , states/f.u./Ry	7.21	6.94	7.07
λ	1.82	1.63	1.44
ω_{log} , K	1362	1511	1675
T_C , K	156	141	118
$\Delta(0)$, meV	29.6	25.7	20.2
$\mu_0 H_C(0)$, T	35.0	29.9	23.6
$\Delta C/T_C$, mJ/mol·K ²	18.6	15.1	12.4
γ , mJ/mol·K ²	7.3	6.5	6.1
$R_\Delta = 2\Delta(0)/k_B T_C$	4.5	4.2	4.0

Table 3 shows the critical temperatures for LaH_{10} and LaH_{16} calculated using the SCDFT and the values of μ^* adjusted so that the Eliashberg and A-D equations give the same values of T_C .

Table 3. Superconducting parameters of LaH_{10} and LaH_{16} phases

Parameter	LaH_{10} at 200 GPa	LaH_{16} at 200 GPa
Critical temperature (T_C), K	271	156
μ^* (Eliashberg eq.)	0.20	0.41
μ^* (Allen–Dynes eq.)	0.11	0.198

IV. Superconductivity of LaH_m ($m = 4, \dots, 9, 11$)

It was shown before that different lanthanum hydrides can undergo a series of superconducting transitions at different pressures with different T_C [1], so we checked other lanthanum hydrides to explore this possibility. In this work, we found a number of LaH_m phases ($m = 4, \dots, 9, 11$) at different pressures, and calculating their T_C using the SCDFT method or the numerical solution of the Eliashberg equation would have been very computationally expensive. Therefore, we calculated T_C of LaH_m phases ($m = 4, \dots, 9, 11$) using the Allen–Dynes (A-D) formula [52, 57] in the pressure range of 150–180 GPa, which is the experimentally studied pressure region [1], with the commonly accepted μ^* values (0.1–0.15). We consider this interval of μ^* reasonable because for LaH_{10} and LaH_{16} the A-D formula yielded μ^* equal to 0.11 and 0.2, respectively (Supporting Information Table S2 [51]). The calculated T_C values are shown in Fig. 4. The results point to LaH_4 , LaH_6 , and LaH_7 as the compounds that could undergo the experimentally observed transition at ~ 215 K with the critical magnetic field $\mu_0 H_C(0) = 60$ –70 T; the other transition at ~ 112 K with the critical magnetic field $\mu_0 H_C(0) = 20$ –25 T could occur in LaH_5 , LaH_8 , and LaH_{11} . More details about the calculation of T_C in these phases can be found in Supporting Information [51].

V. Possible departure from the standard Eliashberg picture

In the present analysis, we estimated the superconducting parameters with the A-D formula and isotropic (constant-DOS) Eliashberg equation. They are based on a simple standard view of the detailed electronic structure such as the constant electronic DOS and screened Coulomb matrix elements. The degree of departure of the target system from this simple view can be estimated by analyzing the Coulomb pseudopotential μ^* [54]. We evaluated the nonrenormalized μ as the Fermi surface average of the screened Coulomb interaction [50, 51], which was 0.18 and 0.11 for LaH_{10} and LaH_{16} , respectively. The straightforward use of the renormalization formula

$$\mu^* = \mu / [1 + \mu \ln(E_{\text{el}}/\omega_D)], \quad (2)$$

where E_{el} is the Fermi level calculated from the band bottom and ω_D is the Debye frequency, yields $\mu^* = 0.10$ and 0.07, which is far smaller than our estimate from the SCDFT results (0.20 and 0.41, respectively). The deviation of μ^* estimated using the SCDFT approach from the empirically accepted range 0.10–0.13 [50, 52] has been pointed out in the previous SCDFT studies [53, 58]. It is thought to indicate the substantial effects ignored in Eq. (2), such as the energy dependence of the electronic DOS and the Kohn–Sham state dependence of the Coulomb matrix element, which are incorporated in the SCDFT framework. Notably, we found a paradoxical relation, $\mu < \mu^*$, derived from the SCDFT, which has also been observed in H_3S [60]. The DOS effect would be accounted for more properly by the DOS-dependent Eliashberg equation [61]. However, the single-parameter approximation of the Coulomb effect is likely less reliable in hydrides because of the large phonon energy scale comparable to the electronic one. The ab initio treatment of the Coulomb matrix element in the Eliashberg equation [62] would reveal such effects on the superconducting parameters evaluated above, which is out of the scope of the present study.

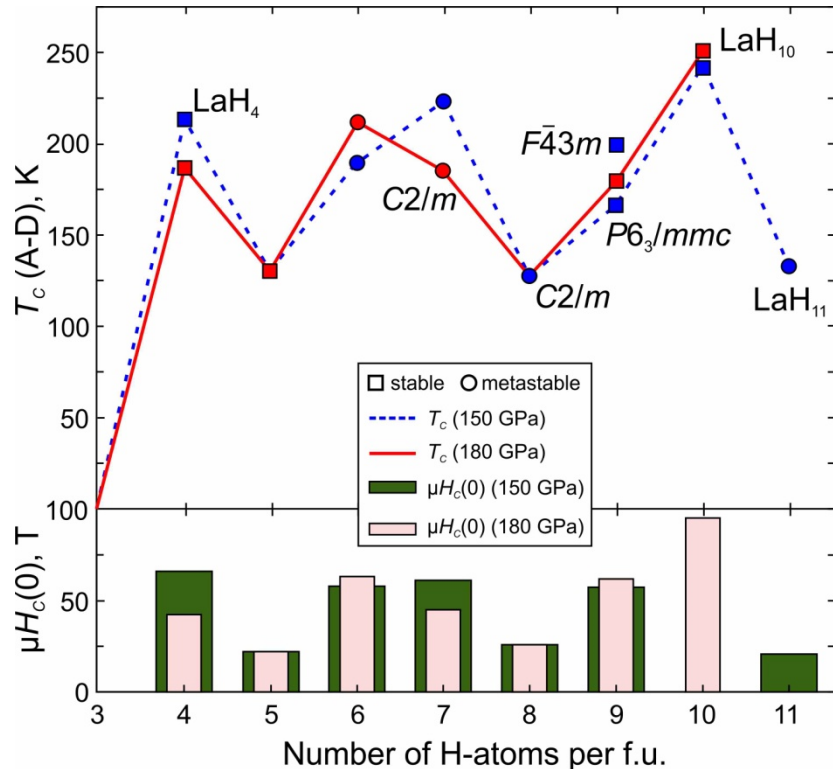


Fig. 4. Superconducting temperatures T_C , obtained using the A-D formula with $\mu^* = 0.1$, and critical magnetic fields for a series of lanthanum hydrides at 150 and 180 GPa.

Conclusions

Using the ab initio evolutionary algorithm USPEX, we predicted stable superconducting compounds in the La-H system at 50, 100, 150, and 200 GPa, including the previously unknown polyhydride $P\bar{6}/mmm$ -LaH₁₆. The electronic, phonon, and superconducting properties of LaH_{*m*} with $m = 4, \dots, 11$ were studied within the harmonic approximation, which gives possible explanations of the observed superconducting transitions at 70, 112, and 215 K [1]. The SCDFT calculations for LaH₁₀ and LaH₁₆ led to unusually high values of μ^* (0.2–0.41) for the numerical solution of the Eliashberg equation, lying far outside the conventionally accepted interval, 0.1–0.15. The Eliashberg function calculated for $Fm\bar{3}m$ -LaH₁₀ at 170 GPa yields $T_C = 259$ K, according to the numerical solution of the Eliashberg equation with $\mu^* = 0.2$. The critical magnetic field of $Fm\bar{3}m$ -LaH₁₀ was found to be 89–95 T (73 T for the $R\bar{3}m$ phase), the harmonic isotope coefficient $\beta = 0.48$. The values of all the superconducting parameters for lanthanum hydrides are in close agreement with the available experimental data [1]. We found that $P\bar{6}/mmm$ -LaH₁₆ is a high-temperature superconductor with T_C of up to 156 K, the critical magnetic field of ~ 35 T, and the superconducting gap of 30 meV at 200 GPa. The main conclusion of this investigation is that even in one system the μ^* value, especially for the numerical solution of the Eliashberg equation, may significantly vary and go beyond the commonly accepted interval, 0.1–0.15, which lends a special importance to the SCDFT calculations.

Acknowledgments

A.R.O. acknowledges the support by the Russian Science Foundation (grant 19-72-30043). A.G.K. thanks the RFBR project № 19-03-00100 and FASIE for the financial support within the UMNIK grant № 13408GU/2018. The calculations were performed on Rurik supercomputer at MIPT and Arkuda supercomputer of the Skolkovo Foundation.

References

[1] A. P. Drozdov, P. P. Kong, V. S. Minkov, S. P. Besedin, M. A. Kuzovnikov, S. Mozaffari,

L. Balicas, F. F. Balakirev, D. E. Graf, V. B. Prakapenka, E. Greenberg, D. A. Knyazev, M. Tkacz, and M. I. Eremets, *Nature* **569**, 528 (2019).

[2] M. Somayazulu, M. Ahart, A. K. Mishra, Z. M. Geballe, M. Baldini, Y. Meng, V. V. Struzhkin, and R. J. Hemley, *Phys. Rev. Lett.* **122**, 027001 (2019).

[3] N. W. Ashcroft, *Phys. Rev. Lett.* **21**, 1748 (1968).

[4] P. Cudazzo, G. Profeta, A. Sanna, A. Floris, A. Continenza, S. Massidda, and E. K. U. Gross, *Phys. Rev. Lett.* **100**, 257001 (2008).

[5] P. Cudazzo, G. Profeta, A. Sanna, A. Floris, A. Continenza, S. Massidda, and E. K. U. Gross, *Phys. Rev. B* **81**, 134505 (2010).

[6] P. Cudazzo, G. Profeta, A. Sanna, A. Floris, A. Continenza, S. Massidda, and E. K. U. Gross, *Phys. Rev. B* **81**, 134506 (2010).

[7] R. P. Dias and I. F. Silvera, *Science* **355**, 715 (2017).

[8] N. W. Ashcroft, *Phys. Rev. Lett.* **92**, 187002 (2004).

[9] H. Wang, J. S. Tse, K. Tanaka, T. Iitaka, and Y. Ma, *Proc. Natl. Acad. Sci.* **109**, 6463 (2012).

[10] H. Liu, I. I. Naumov, R. Hoffmann, N. W. Ashcroft, and R. J. Hemley, *Proc. Natl. Acad. Sci.* **114**, 6990 (2017).

[11] D. Duan, Y. Liu, F. Tian, D. Li, X. Huang, Z. Zhao, H. Yu, B. Liu, W. Tian, and T. Cui, *Sci. Rep.* **4**, 6968 (2014).

[12] A. G. Kvashnin, D. V. Semenok, I. A. Kruglov, I. A. Wrona, and A. R. Oganov, *ACS Appl. Mater. Interfaces* **10**, 43809 (2018).

[13] D. V. Semenok, A. G. Kvashnin, I. A. Kruglov, and A. R. Oganov, *J. Phys. Chem. Lett.* **9**, 1920 (2018).

[14] W. Zhang, A. R. Oganov, A. F. Goncharov, Q. Zhu, S. E. Boulfelfel, A. O. Lyakhov, M. Somayazulu, and V. B. Prakapenka, *Science* **342**, 1502 (2013).

[15] A. P. Drozdov, M. I. Eremets, I. A. Troyan, V. Ksenofontov, and S. I. Shylin, *Nature* **525**, 73 (2015).

[16] I. A. Kruglov, A. G. Kvashnin, A. F. Goncharov, A. R. Oganov, S. S. Lobanov, N. Holtgrewe, Sh. Jiang, V. B. Prakapenka, E. Greenberg, and A. V. Yanilkin, *Sci Adv* **4**, eaat9776 (2018).

[17] D. Duan, Y. Liu, Y. Ma, Z. Shao, B. Liu, and T. Cui, *Natl. Sci. Rev.* **4**, 121 (2017).

[18] A. K. Mishra, M. Somayazulu, M. Ahart, A. Karandikar, R. J. Hemley, and V. V. Struzhkin, in *Bull. Am. Phys. Soc.* (2018).

[19] P. P. Kong, A. P. Drozdov, E. Eroke, and M. I. Eremets, in *Book Abstr. AIRAPT 26 Jt. ACHPR 8 CHPC 19* (Beijing, China, 2017), p. 347.

[20] Z. M. Geballe, H. Liu, A. K. Mishra, M. Ahart, M. Somayazulu, Y. Meng, M. Baldini, and R. J. Hemley, *Angew. Chem. Int. Ed.* **57**, 688 (2017).

[21] C. M. Pépin, G. Geneste, A. Dewaele, M. Mezouar, and P. Loubeyre, *Science* **357**, 382 (2017).

[22] A. Majumdar, J. S. Tse, M. Wu, and Y. Yao, *Phys. Rev. B* **96**, 201107 (2017).

[23] A. G. Kvashnin, I. A. Kruglov, D. V. Semenok, and A. R. Oganov, *J. Phys. Chem. C* **122**, 4731 (2018).

[24] N. P. Salke, M. M. D. Esfahani, Y. Zhang, I. A. Kruglov, J. Zhou, Y. Wang, E. Greenberg, V. B. Prakapenka, A. R. Oganov, and J.-F. Lin, ArXiv:1805.02060
<https://arxiv.org/ftp/arxiv/papers/1805/1805.02060.pdf> (2018).

[25] H. Wang, J. S. Tse, K. Tanaka, T. Iitaka, and Y. Ma, *Proc. Natl. Acad. Sci.* **109**, 6463 (2012).

[26] K. Tanaka, J. S. Tse, and H. Liu, *Phys. Rev. B* **96**, 100502 (2017).

[27] G. Gao, R. Hoffmann, N. W. Ashcroft, H. Liu, A. Bergara, and Y. Ma, *Phys. Rev. B* **88**, 184104 (2013).

[28] K. Abe, *Phys. Rev. B* **96**, 144108 (2017).

[29] X. Li and F. Peng, *Inorg. Chem.* **56**, 13759 (2017).

- [30] A. R. Oganov and C. W. Glass, *J Chem Phys* **124**, 244704 (2006).
- [31] A. R. Oganov, A. O. Lyakhov, and M. Valle, *Acc. Chem. Res.* **44**, 227 (2011).
- [32] A. O. Lyakhov, A. R. Oganov, H. T. Stokes, and Q. Zhu, *Comput. Phys. Commun.* **184**, 1172 (2013).
- [33] P. V. Bushlanov, V. A. Blatov, and A. R. Oganov, *Comput. Phys. Commun.* **236**, 1 (2019).
- [34] P. Hohenberg and W. Kohn, *Phys Rev* **136**, B864 (1964).
- [35] W. Kohn and L. J. Sham, *Phys Rev* **140**, A1133 (1965).
- [36] J. P. Perdew, K. Burke, and M. Ernzerhof, *Phys. Rev. Lett.* **77**, 3865 (1996).
- [37] P. E. Blöchl, *Phys. Rev. B* **50**, 17953 (1994).
- [38] G. Kresse and D. Joubert, *Phys. Rev. B* **59**, 1758 (1999).
- [39] G. Kresse and J. Furthmüller, *Phys. Rev. B* **54**, 11169 (1996).
- [40] G. Kresse and J. Hafner, *Phys. Rev. B* **47**, 558 (1993).
- [41] G. Kresse and J. Hafner, *Phys. Rev. B* **49**, 14251 (1994).
- [42] P. Giannozzi, S. Baroni, N. Bonini, M. Calandra, R. Car, C. Cavazzoni, D. Ceresoli, G. L. Chiarotti, M. Cococcioni, I. Dabo, A. D. Corso, S. de Gironcoli, S. Fabris, G. Fratesi, R. Gebauer, U. Gerstmann, C. Gougaussis, A. Kokalj, M. Lazzeri, L. Martin-Samos, N. Marzari, F. Mauri, R. Mazzarello, S. Paolini, A. Pasquarello, L. Paulatto, C. Sbraccia, S. Scandolo, G. Sclauzero, A. P. Seitsonen, A. Smogunov, P. Umari, and R. M. Wentzcovitch, *J. Phys. Condens. Matter* **21**, 395502 (2009).
- [43] S. Baroni, S. de Gironcoli, A. Dal Corso, and P. Giannozzi, *Rev. Mod. Phys.* **73**, 515 (2001).
- [44] A. Togo and I. Tanaka, *Scr. Mater.* **108**, 1 (2015).
- [45] A. Togo, F. Oba, and I. Tanaka, *Phys. Rev. B* **78**, 134106 (2008).
- [46] M. Lüders, M. A. L. Marques, N. N. Lathiotakis, A. Floris, G. Profeta, L. Fast, A. Continenza, S. Massidda, and E. K. U. Gross, *Phys. Rev. B* **72**, 024545 (2005).
- [47] M. A. L. Marques, M. Lüders, N. N. Lathiotakis, G. Profeta, A. Floris, L. Fast, A. Continenza, E. K. U. Gross, and S. Massidda, *Phys. Rev. B* **72**, 024546 (2005).
- [48] R. Akashi and R. Arita, *Phys. Rev. B* **88**, 014514 (2013).
- [49] R. Akashi, M. Kawamura, S. Tsuneyuki, Y. Nomura, and R. Arita, *Phys. Rev. B* **91**, 224513 (2015).
- [50] P. Morel and P. W. Anderson, *Phys. Rev.* **125**, 1263 (1962).
- [51] See Supplemental Material at [URL will be inserted by the production group] for crystal data of La-H phases, electronic, phonon and superconducting properties including Eliashberg spectral functions, (n.d.).
- [52] K.-H. Lee, K. J. Chang, and M. L. Cohen, *Phys. Rev. B* **52**, 1425 (1995).
- [53] J. P. Carbotte, *Rev. Mod. Phys.* **62**, 1027 (1990).
- [54] G. Profeta, C. Franchini, N. N. Lathiotakis, A. Floris, A. Sanna, M. A. L. Marques, M. Lüders, S. Massidda, E. K. U. Gross, and A. Continenza, *Phys. Rev. Lett.* **96**, 047003 (2006).
- [55] F. Peng, Y. Sun, C. J. Pickard, R. J. Needs, Q. Wu, and Y. Ma, *Phys. Rev. Lett.* **119**, 107001 (2017).
- [56] D. V. Semenok, I. A. Kruglov, A. G. Kvashnin, and A. R. Oganov, *ArXiv* (2018).
- [57] K. Momma and F. Izumi, *J. Appl. Crystallogr.* **44**, 1272 (2011).
- [58] P. B. Allen and R. C. Dynes, *Phys. Rev. B* **12**, 905 (1975).
- [59] R. Akashi, K. Nakamura, R. Arita, and M. Imada, *Phys. Rev. B* **86**, 054513 (2012).
- [60] J. Flores-Livas, A. Sanna, and E. K. U. Gross, *Eur. Phys. J. B* **89**, 63 (2016).
- [61] W. E. Pickett, *Phys. Rev. B* **26**, 1186 (1982).
- [62] A. Sanna, J. A. Flores-Livas, A. Davydov, G. Profeta, K. Dewhurst, S. Sharma, and E. K. U. Gross, *J. Phys. Soc. Jpn.* **87**, 041012 (2018).

Supporting Information

Superconductivity in LaH₁₀ and LaH₁₆ polyhydrides

Ivan A. Kruglov,^{1,2,} Dmitrii V. Semenok,^{1,3} Hao Song⁹, Radosław Szczęśniak,^{4,5} Izabela A. Wrona,⁴ Ryosuke Akashi,⁶ M. Mahdi Davari Esfahani,⁷ Defang Duan,⁹ Tian Cui,⁹ Alexander G. Kvashnin^{3,1} and Artem R. Oganov^{3,2,8}*

¹ Moscow Institute of Physics and Technology, 141700, 9 Institutsky lane, Dolgoprudny, Russia

² Dukhov Research Institute of Automatics (VNIIA), Moscow 127055, Russia

³ Skolkovo Institute of Science and Technology, Skolkovo Innovation Center 143026, 3 Nobel Street, Moscow, Russia

⁴ Institute of Physics, Jan Dlugosz University in Czestochowa, Ave. Armii Krajowej 13/15, 42-200 Czestochowa, Poland

⁵ Institute of Physics, Czestochowa University of Technology, Ave. Armii Krajowej 19, 42-200 Czestochowa, Poland

⁶University of Tokyo, 7-3-1 Hongo, Bunkyo, Tokyo 113-8654, Japan

⁷ Department of Geosciences and Center for Materials by Design, Institute for Advanced Computational Science, State University of New York, Stony Brook, NY 11794-2100, USA

⁸ International Center for Materials Discovery, Northwestern Polytechnical University, Xi'an, 710072, China

⁹Key State Laboratory of Superhard Materials, Jilin University, Changchun, China

Corresponding Author

*Ivan A. Kruglov, E-mail: ivan.kruglov@phystech.edu

*Dmitrii V. Semenok, E-mail: Dmitrii.Semenok@skoltech.ru

*Artem. R. Oganov, E-mail: A.Oganov@skoltech.ru

Content

Content

Crystal data of La-H phases	S2
Equations for calculating T_c and related parameters.....	S3
Calculation of critical magnetic field for LaH ₁₀ phases.....	S9
Superconductivity of lanthanum hydrides LaH _{m} ($m = 4-9, 11$).....	S10
Electronic and phonon properties of La-H phases	S12
Eliashberg spectral functions	S17
Stability of LaH ₁₀ polymorphs.....	S20
References.....	S21

Crystal data of La-H phases

Table S1. Crystal structures of predicted La-H phases.

Phase	Pressure, GPa	Lattice parameters	Coordinates			
<i>Fm</i> $\bar{3}m$ -LaH	50	a = 4.53 Å	La	0.5	0.5	0.5
			H	0.0	0.0	0.0
<i>Pnma</i> -LaH ₃	50	a = 7.20 Å, b = 4.57 Å, c = 3.67 Å	La	-0.365	0.25	-0.320
			H	0.394	-0.001	-0.171
			H	0.356	0.25	0.332
<i>Cmc2</i> ₁ -LaH ₇	50	a = 7.20 Å, b = 4.57 Å, c = 3.67 Å	La	0.0	-0.159	-0.452
			H	0.0	0.466	0.408
			H	0.0	0.245	-0.300
			H	0.0	-0.365	0.241
			H	0.0	0.174	0.420
			H	0.25	0.417	0.237
			H	0.0	-0.497	-0.465
<i>P6/mmm</i> -LaH ₂	150	a = 2.80 Å, c = 2.72 Å	La	0.0	0.0	0.0
			H	0.333	0.667	0.5
<i>Cmcm</i> -LaH ₃	150	a = 2.76 Å, b = 10.69 Å, c = 2.80 Å	La	0.0	0.118	0.25
			H	0.0	0.467	0.25
			H	0.0	0.313	0.25
			H	0.0	-0.25	0.25
<i>Cmmm</i> -La ₃ H ₁₀	150	a = 16.70 Å, b = 2.77 Å, c = 2.75 Å	La	-0.326	0.0	0.5
			La	0.0	0.0	0.0
			H	-0.089	0.0	0.5
			H	0.128	0.0	0.0
			H	-0.228	0.0	0.0
			H	-0.449	0.0	0.5
			H	0.411	0.0	0.0
<i>I4/mmm</i> -LaH ₄	150	a = 2.74 Å, c = 6.03 Å	La	0.0	0.0	0.5
			H	0.0	0.5	0.25
			H	0.0	0.0	-0.153
<i>P</i> $\bar{1}$ -LaH ₅	150	a = 2.91 Å, b = 5.26 Å, c = 3.47 Å, α = 93.34, β = 110.24, γ = 98.71	La	-0.327	-0.266	-0.273
			H	0.263	0.036	-0.255
			H	0.073	0.431	-0.280
			H	-0.067	0.122	-0.349
			H	-0.304	0.375	-0.108
			H	-0.376	0.112	-0.151
<i>R</i> $\bar{3}m$ -LaH ₁₀	150	a = 3.66 Å, c = 8.53 Å	La	0.0	0.0	0.5
			H	0.0	0.0	0.097
			H	-0.168	0.168	0.276
			H	0.0	0.0	-0.259
<i>Fm</i> $\bar{3}m$ -LaH ₁₀	150	a = 5.08 Å	La	0.0	0.0	0.0
			H	-0.378	-0.378	-0.378
			H	0.25	0.25	0.25
<i>P6/mmm</i> -LaH ₁₆	150	a = 3.68 Å, c = 3.70 Å	La	0.0	0.0	0.0
			H	-0.276	0.0	0.5
			H	0.5	0.0	0.245
			H	0.333	0.667	-0.203

Equations for calculating T_c and related parameters

The superconducting transition temperature was calculated by solving the gap equation derived from the density functional theory for superconductors (SCDFT) [1,2], where no empirical parameter such as μ^* was used. The nk -averaged formula for K^{ph} [Eq.(23) in Ref. [2]] and Z^{ph} [Eq.(40) in Ref. [3]] were employed to use the calculated $\alpha^2 F(\omega)$. The nk -dependent formula for K^{ph} [Eq.(3) in Ref. [4]] was used, which includes the dynamical as well as static screening effect on the Coulomb repulsion. The dielectric matrices $\epsilon(i\omega)$ were represented with the auxiliary plane-wave energy cutoff of 12.8 Ry and were calculated within the random-phase approximation [5] and electron-electron Coulomb matrix elements were evaluated as

$$W_{nk,n'k'}(i\omega) = \langle \psi_{nk} \psi_{n-k} | \epsilon^{-1}(i\omega) V | \psi_{n'k'} \psi_{n'-k'} \rangle \quad (\text{S1})$$

where V is being the bare Coulomb interaction. Low-energy Kohn-Sham states were accurately treated with the weighted random sampling scheme in solving the gap equation, as described in Ref. [2]. The Kohn-Sham energy eigenvalues and matrix elements for the sampled states were evaluated by the linear interpolation from the data on equal meshes. The detailed conditions are summarized in Table S2.

Table S2. Summary of the detailed conditions for the T_c calculation with the SCDFT scheme.

Class	Parameter	LaH ₁₀ 200GPa	LaH ₁₆ 200GPa
charge density	k	16x16x16 equal mesh	16x16x16 equal mesh
	interpolation	1st order Hermite Gaussian [5] with width 0.050Ry	
dielectric matrix	k for bands crossing E_F	15x15x15 equal mesh	15x15x15 equal mesh
	k for other bands	5x5x5 equal mesh	5x5x5 equal mesh
	number of unoccupied bands ^a	57	75
	interpolation	Tetrahedron with the Rath-Freeman treatment [6]	
DOS for phononic kernels	k	21x21x21 equal mesh	21x21x21 equal mesh
	interpolation	Tetrahedron with the Blöchl correction [7]	
SCDFT gap function	number of unoccupied bands ^b	24	36
	k for the electronic kernel	5x5x5 equal mesh	5x5x5 equal mesh
	k for the KS energies	21x21x21 equal mesh	21x21x21 equal mesh
	Sampling points for bands crossing E_F	6000	6000
	Sampling points for the other bands	200	200
	Sampling error in T_c (%)	~2.6	~1.9
SC parameters	Critical temperature (T_c)	271	156
	Coloumb pseudopotential μ^* (E) μ^* (Allen-Dynes)	0.20 0.11	0.41 0.198

^a States up to $E_F+70\text{eV}$ are taken into account.

^b States up to $E_F+40\text{eV}$ are taken into account.

Isotopic coefficient β_{AD} was calculated using the Allen-Dynes interpolation formulas:

$$\beta_{McM} = -\frac{d \ln T_C}{d \ln M} = \frac{1}{2} \left[1 - \frac{1.04(1+\lambda)(1+0.62\lambda)}{[\lambda - \mu^*(1+0.62\lambda)]^2} \mu^{*2} \right] \quad (S2)$$

$$\beta_{AD} = \beta_{McM} - \frac{2.34\mu^{*2}\lambda^{3/2}}{(2.46+9.25\mu^*) \cdot ((2.46+9.25\mu^*)^{3/2} + \lambda^{3/2})} - \frac{130.4 \cdot \mu^{*2} \lambda^2 (1+6.3\mu^*) \left(1 - \frac{\omega_{\log}}{\omega_2} \right) \frac{\omega_{\log}}{\omega_2}}{\left(8.28+104\mu^* + 329\mu^{*2} + 2.5 \cdot \lambda^2 \frac{\omega_{\log}}{\omega_2} \right) \cdot \left(8.28+104\mu^* + 329\mu^{*2} + 2.5 \cdot \lambda^2 \left(\frac{\omega_{\log}}{\omega_2} \right)^2 \right)} \quad (S3)$$

where the last two correction terms are usually small (~ 0.01).

The critical temperature of superconducting transition was calculated using Matsubara-type linearized Eliashberg equations: [8]

$$\hbar\omega_j = \pi(2j+1) \cdot k_B T, \quad j = 0, \pm 1, \pm 2, \dots \quad (S4)$$

$$\lambda(\omega_i - \omega_j) = 2 \int_0^{\infty} \frac{\omega \cdot \alpha^2 F(\omega)}{\omega^2 + (\omega_i - \omega_j)^2} d\omega \quad (S5)$$

$$\Delta(\omega = \omega_i, T) = \Delta_i(T) = \pi k_B T \sum_j \frac{[\lambda(\omega_i - \omega_j) - \mu^*]}{\rho + \left| \hbar\omega_j + \pi k_B T \sum_k (sign \omega_k) \cdot \lambda(\omega_j - \omega_k) \right|} \cdot \Delta_j(T), \quad (S6)$$

where T is temperature in Kelvins, μ^* is Coloumb pseudopotential, ω is frequency in Hz, $\rho(T)$ is a pair-breaking parameter, function $\lambda(\omega_i - \omega_j)$ relates to effective electron-electron interaction via exchange of phonons. [9] Transition temperature can be found as a solution of equation $\rho(T_C) = 0$ where $\rho(T)$ is defined as $max(\rho)$ providing that $\Delta(\omega)$ is not a zero function of ω at fixed temperature.

These equations can be rewritten in a matrix form as [10]

$$\rho(T) \psi_m = \sum_{n=0}^N K_{mn} \psi_n \Leftrightarrow \rho(T) \begin{pmatrix} \psi_1 \\ \dots \\ \psi_N \end{pmatrix} = \begin{pmatrix} K_{11} & \dots & K_{1N} \\ \dots & K_{ii} & \dots \\ K_{N1} & \dots & K_{NN} \end{pmatrix} \times \begin{pmatrix} \psi_1 \\ \dots \\ \psi_N \end{pmatrix}, \quad (S7)$$

where ψ_n relates to $\Delta(\omega, T)$, and

$$K_{mn} = F(m-n) + F(m+n+1) - 2\mu^* - \delta_{mn} \left[2m+1 + F(0) + 2 \sum_{l=1}^m F(l) \right] \quad (S8)$$

$$F(x) = F(x, T) = 2 \int_0^{\omega_{\max}} \frac{\alpha^2 F(\omega)}{(\hbar\omega)^2 + (2\pi \cdot kT \cdot x)^2} \hbar^2 \omega d\omega, \quad (S9)$$

where $\delta_{nn} = 1$ and $\delta_{nm} = 0$ ($n \neq m$) – is a unit matrix. Now one can replace criterion of $\rho(T_C) = 0$ by the vanishing of the maximum eigenvalue of the matrix K_{nm} : $\{\rho = max_eigenvalue(K_{nm}) = f(T), f(T_C) = 0\}$.

We have implemented this simple approach, proposed by Philip Allen in 1974, as Matlab functions, shown at the last page of Supporting Information, which read files with α^2F functions and carry out the calculations of T_C .

Exact calculations for $P6/mmm$ -LaH₁₆ at 250 GPa were also made using the Eliashberg equations in the following form (on the imaginary axis) [8]:

$$\phi_n = \frac{\pi}{\beta} \sum_{m=-M}^M \frac{\lambda(i\omega_n - i\omega_m) - \mu^* \theta(\omega_c - |\omega_m|)}{\sqrt{(\hbar\omega_m Z_m)^2 + \phi_m^2}} \phi_m \quad (S10)$$

$$Z_n = 1 + \frac{1}{\omega_n} \frac{\pi}{\beta} \sum_{m=-M}^M \frac{\lambda(i\omega_n - i\omega_m)}{\sqrt{(\hbar\omega_m Z_m)^2 + \phi_m^2}} \omega_m Z_m \quad (S11)$$

where: ϕ_n is the order parameter function, Z_n is the wave function renormalization factor, $\theta(x)$ is Heaviside function, $\hbar\omega_n = \pi \cdot k_B T \cdot (2n-1)$ is the n -th Matsubara frequency, $\beta = 1/k_B T$, μ^* is Coulomb pseudopotential, ω_c is the cut-off energy ($\omega_c = 3\Omega_{\max}$, Ω_{\max} is the maximum frequency in $\alpha^2F(\omega)$). The electron-phonon pairing kernel is defined as:

$$\lambda(z) = 2 \int_0^{\Omega_{\max}} \frac{\alpha^2 F(\Omega)}{\Omega^2 - z^2} \Omega d\Omega. \quad (S12)$$

The Eliashberg equations were solved for 2201 Matsubara frequencies, starting from $T_0 = 10$ K (below this temperature, the solutions are not stable). The methods discussed in the papers [11–13] were used during the calculations.

The full form of the order parameter and the wave function renormalization factor on the real axis was obtained through analytical extension of the Eliashberg equations solutions from the imaginary axis, using the formula:

$$X(\omega) = \frac{p_1 + p_2 \omega + \dots + p_r \omega^{r-1}}{q_1 + q_2 \omega + \dots + q_r \omega^{r-1} + \omega^r}, \quad (S13)$$

where $X \in \{\Delta; Z\}$, $r = 50$. The values of p_j and q_j parameters were selected in accordance with the principles presented in work [14]. Obtained results allow one to calculate dimensionless parameter R_C (relative jump of the specific heat), using the formula below:

$$R_C = \frac{C^S(T_C) - C^N(T_C)}{C^N(T_C)} \quad (S14)$$

Because of strong-coupling and retardation effects in LaH₁₀ and LaH₁₆, parameter R_C differs significantly from BCS theory prediction, in which the constant value is equal to 1.43. [15]

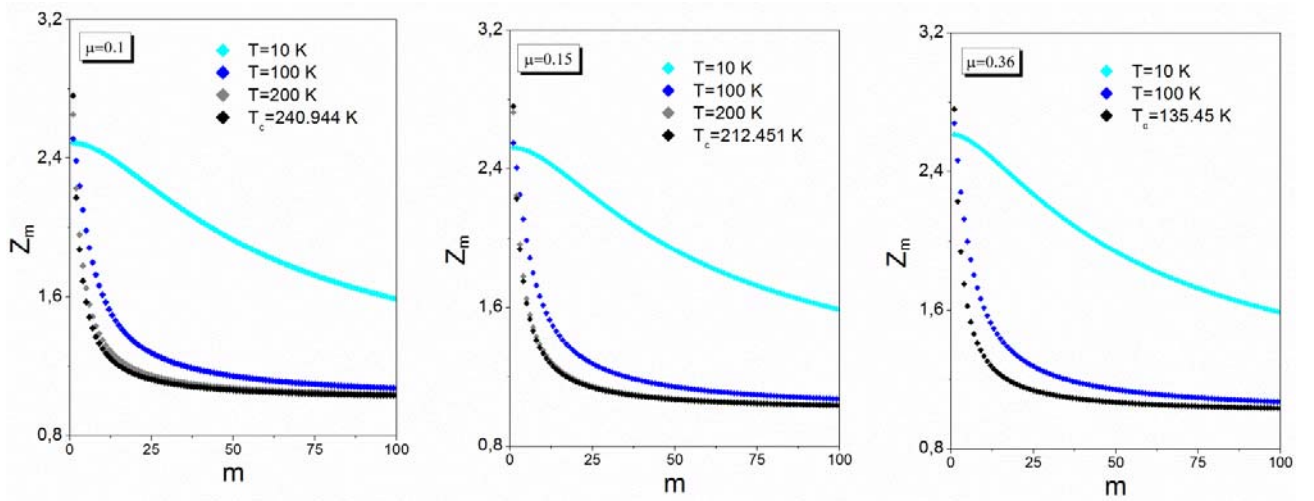


Fig. S1. The wave function renormalization factor for $P6/mmm$ -LaH₁₆ at 250 GPa on the imaginary axis for the selected values of temperature (the first 100 values).

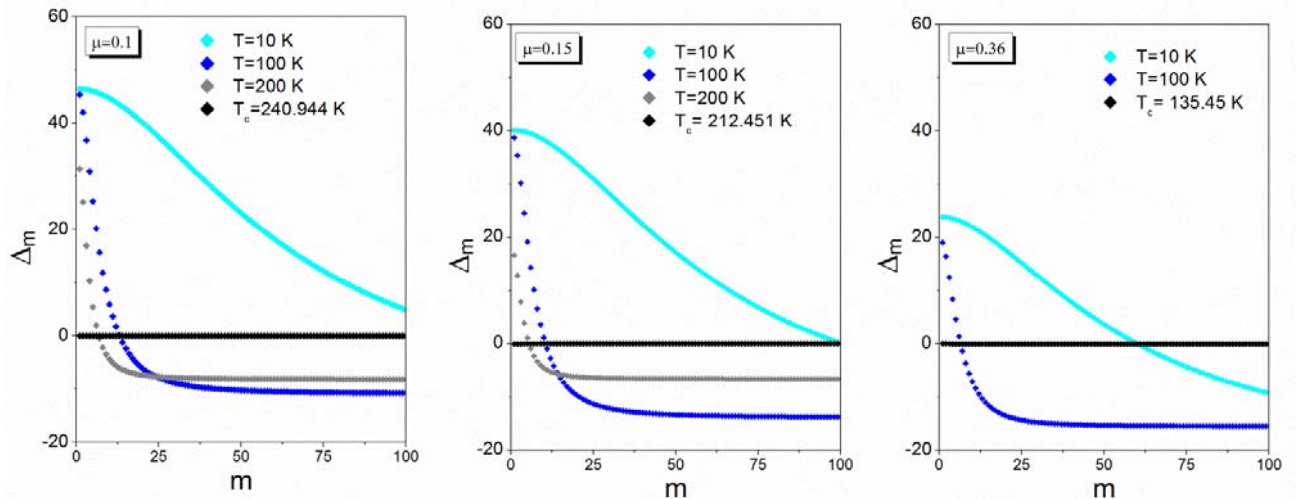


Fig. S2. The order parameter (in meV) for $P6/mmm$ -LaH₁₆ at 250 GPa on the imaginary axis for the selected values of temperature (the first 100 values) and Coulomb pseudopotential.

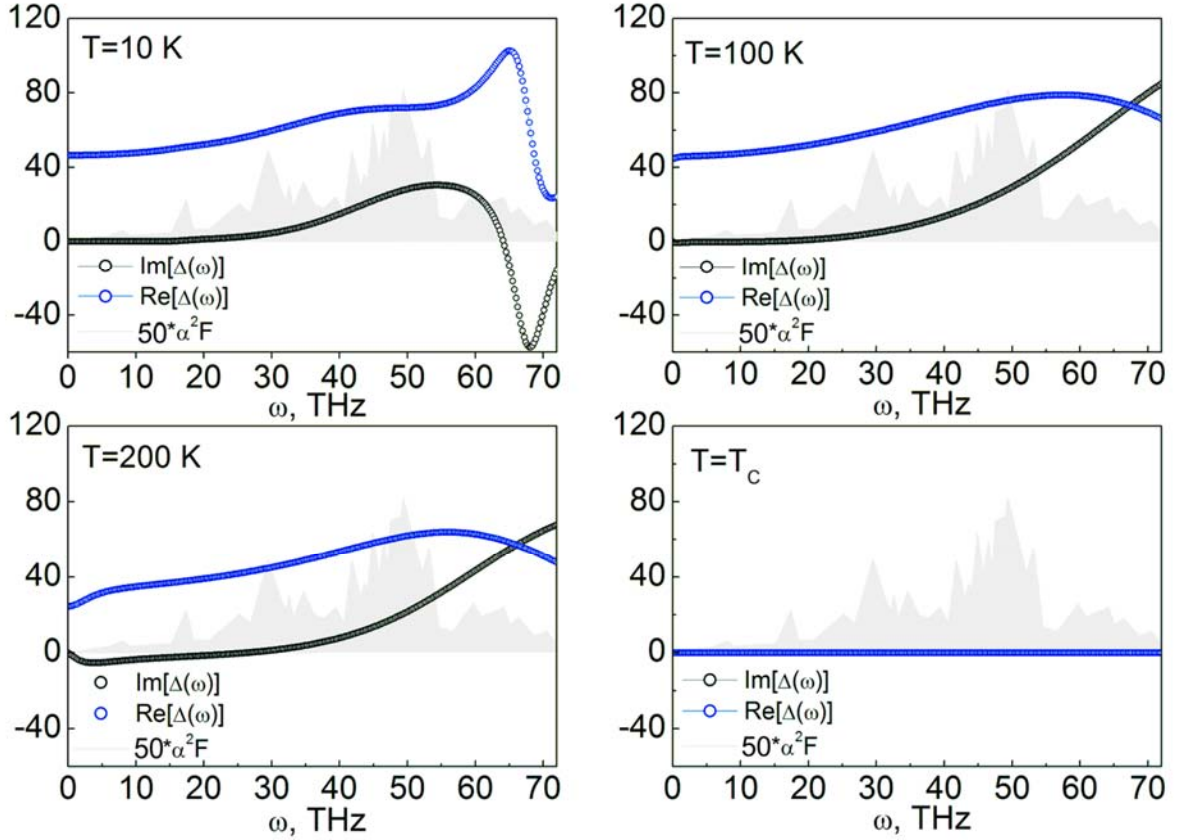


Fig. S3. The order parameter $\Delta(\omega)$ in meV for $P6/mmm$ -LaH₁₆ at 250 GPa on the real axis for the selected values of temperature ($\mu^* = 0.1$). In addition, the Eliashberg function (grey) was added as the background (multiplied by 50 for easier comparison).

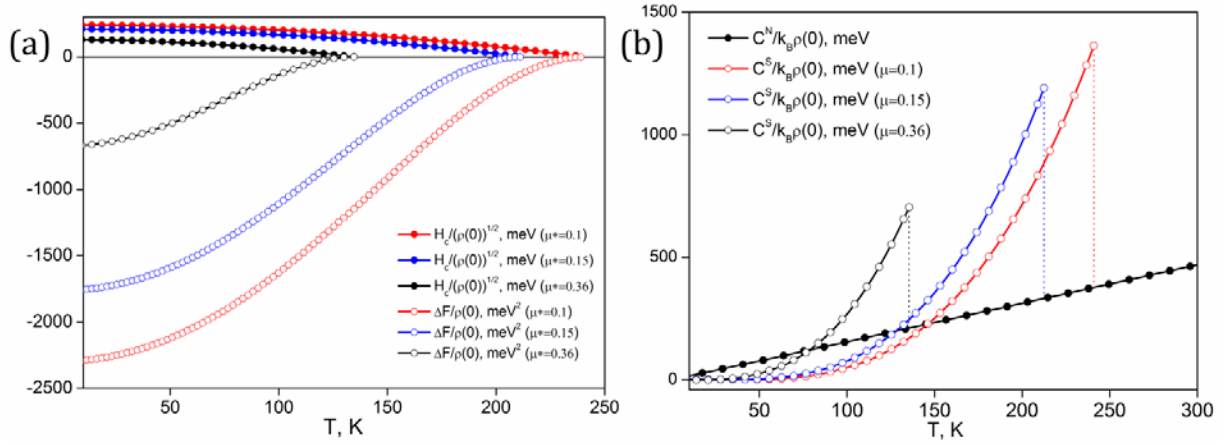


Fig. S4. a) The dependence of the thermodynamic critical field on the temperature (in meV, solid circles) and free energy difference between the superconducting state and the normal state as a function of the temperature (in meV², open circles); b) The specific heat of the superconducting state (C_s) and the normal state (C_N) as a function of temperature. Here $\rho(0)$ is the density of states at the Fermi level.

Table S3. Parameters of superconductive state of $P6/mmm$ -LaH₁₆ at 250 GPa calculated by the Eliashberg equations at different μ^*

Parameter	$P6/mmm$ -LaH ₁₆ (250 GPa)		
	$\mu^*=0.1$	$\mu^*=0.15$	$\mu^*=0.36$
T_C , K	241	213	135
$\Delta(0)$, meV	46.4	40.1	23.9
$\mu_0 H_c(0)$, T	52.3	45.8	28.4
$\Delta C/T_C$, mJ/mol·K ²	17.3	17.2	15.4
γ , mJ/mol·K ²	6.3	6.3	6.3
$R_A = 2\Delta(0)/k_B T_C$	4.47	4.38	4.09

The Sommerfeld constant was calculated using the following formula:

$$\gamma = \frac{2}{3} \pi^2 k_B^2 N(0)(1 + \lambda), \quad (S15)$$

where λ is the EPC parameter, $N(0)$ – the electronic density of states at the Fermi level, k_B – the Boltzmann constant.

Calculation of critical magnetic field for LaH_{10} phases

Using semi-empirical formulas of BCS theory (see Ref. [16], eq. 5.11 and 5.9):

$$\frac{\gamma T_c^2}{H_c^2(0)} = 0.168 \left[1 - 12.2 \left(\frac{T_c}{\omega_{\log}} \right)^2 \ln \left(\frac{\omega_{\log}}{3T_c} \right) \right] \quad (\text{S16})$$

and

$$\frac{\Delta C(T_c)}{\gamma T_c} = 1.43 \left[1 + 53 \left(\frac{T_c}{\omega_{\log}} \right)^2 \ln \left(\frac{\omega_{\log}}{3T_c} \right) \right], \quad (\text{S17})$$

we estimated the critical magnetic field and the jump in specific heat for $Fm\bar{3}m$ - LaH_{10} in harmonic approximation (see Table 2). The superconducting gap was estimated by well-known semi-empirical equation, working satisfactorily for $T_c/\omega_{\log} < 0.25$ (see equation 4.1 in Ref. [16]):

$$\frac{2\Delta(0)}{k_B T_c} = 3.53 \left[1 + 12.5 \left(\frac{T_c}{\omega_{\log}} \right)^2 \ln \left(\frac{\omega_{\log}}{2T_c} \right) \right] \quad (\text{S18})$$

Estimation of the critical magnetic field for $Fm\bar{3}m$ - LaH_{10} gives $\mu_0 H_c(0) \sim 89\text{-}95$ T at 170-200 GPa, which is greater than 70 T for H_3S [17] and agrees with lower bound of recent experimental results of 95-136 T [18].

Superconductivity of lanthanum hydrides LaH_m ($m = 4-9, 11$)

According to Ref. [18], pure LaH_3 is not a superconductor at all investigated pressures (0-200 GPa), but higher hydrides of La are metallic and superconducting. Superconducting properties of all predicted hydrides were computed by Allen-Dynes (A-D) formula [19,16] at the pressure range 150-180 GPa, which is the experimentally studied pressure region [18].

Surprisingly, $I4/mmm$ - LaH_4 demonstrates **very** relatively strong electron-phonon coupling (see Table S4). At 150 GPa the T_C (A-D) is found to be 87 K and it decreases to 67 K at 180 GPa with $dT_C/dP \approx -0.67$ K/GPa. Thus, $I4/mmm$ - LaH_4 could explain superconducting transitions with $T_C = 70-112$ K observed in Ref. [18].

$P\bar{1}$ - LaH_5 is stable at pressures above 150 GPa (Fig. 1c) and has T_C of 104-130 K at 150 GPa (see Table S4), almost insensitive to pressure ($dT_C/dP \approx -0.033$ K/GPa). This could explain the superconducting transition observed at $T_C \sim 112$ K [18].

$R\bar{3}m$ - LaH_6 is metastable, but at 150 GPa it is very close to the convex hull (only 6 meV/atom above it, see Fig. 1c). Its electronic density of states is approximately pressure-independent, and its T_C increases with pressure ($dT_C/dP \approx +0.73$ K/GPa), because of the increase of the characteristic phonon frequency ~~with pressure~~. According to our calculations, T_C of this phase can reach 211 K at 180 GPa (see Table S4).

Table S4. Predicted superconducting properties of slightly metastable and stable lanthanum hydrides. μ^* was taken as 0.1 (0.15).

Phase	P , GPa	λ	N_f states/f.u./Ry	ω_{log} , K	T_C (A-D), K	$\mu_0 H_C(0)$, T
$I4/mmm$ - LaH_4 ^{b)}	150	1.28	8.43	796	87 (69)	25 (22)
	180	0.84	7.62	1255	69 (48)	16 (13)
$P\bar{1}$ - LaH_5 ^{b)}	150	1.21	5.57 ^{a)}	1307	130 (104)	22 (17)
	180	1.15		1389	129 (102)	
$R\bar{3}m$ - LaH_6	150	2.89	9.04 ^{a)}	765	189 (163)	58 (51)
	180	2.60		956	211 (183)	63 (55)
$C2/m$ - LaH_7	150	2.94	7.21	894	223 (193)	61 (54)
	180	1.92	7.55	1102	185 (158)	45 (38)
$C2/m$ - LaH_8 ^{c)}	150	1.56	6.32 ^{a)}	944	128 (107)	26 (21)
	180	1.53		950	127 (106)	
$P6_3/mmc$ - LaH_9	150	2.75	11.6 ^{a)}	702	166 (144)	57 (50)
	180	2.98		708	180 (156)	62 (55)
$F\bar{4}3m$ - LaH_9	150	2.92	7.72	802	199 (172)	56 (49)
$P4/nmm$ - LaH_{11}	150	1.54	3.94	986	133 (111)	21 (17)

a) no changes with pressure; b) stable phase; c) from Ref. [20].

$C2/m$ - LaH_7 is also metastable (17 meV/atom above the convex hull at 150 GPa, Fig. 1c) and displays T_C up to 223 K (with $dT_C/dP \approx -1.26$ K/GPa), see Table 3. This phase may be responsible for observed transition at ~ 215 K [18]. Metastable $C2/m$ - LaH_8 , proposed in Ref. [20], has $T_C = 106-127$ K (Table S4), which is almost insensitive to pressure.

For metastable LaH_9 we considered two polymorphs: isostructural to recently found $P6_3/mmc$ - CeH_9 [21] and $F\bar{4}3m$ - UH_9 [22]. We predict $T_C = 144-166$ K (150 GPa, Table S4) for hexagonal

modification with $dT_C/dP = +0.46$ K/GPa. Obtained value is higher than that for CeH₉ [21,23]. For cubic LaH₉ T_C is higher: up to 199 K at 150 GPa (Table S4).

Metastable *P4/nmm*-LaH₁₁ at 150-180 GPa shows relatively low $T_C = 111$ -133 K (due to low density of states at Fermi level).

Electronic and phonon properties of La-H phases

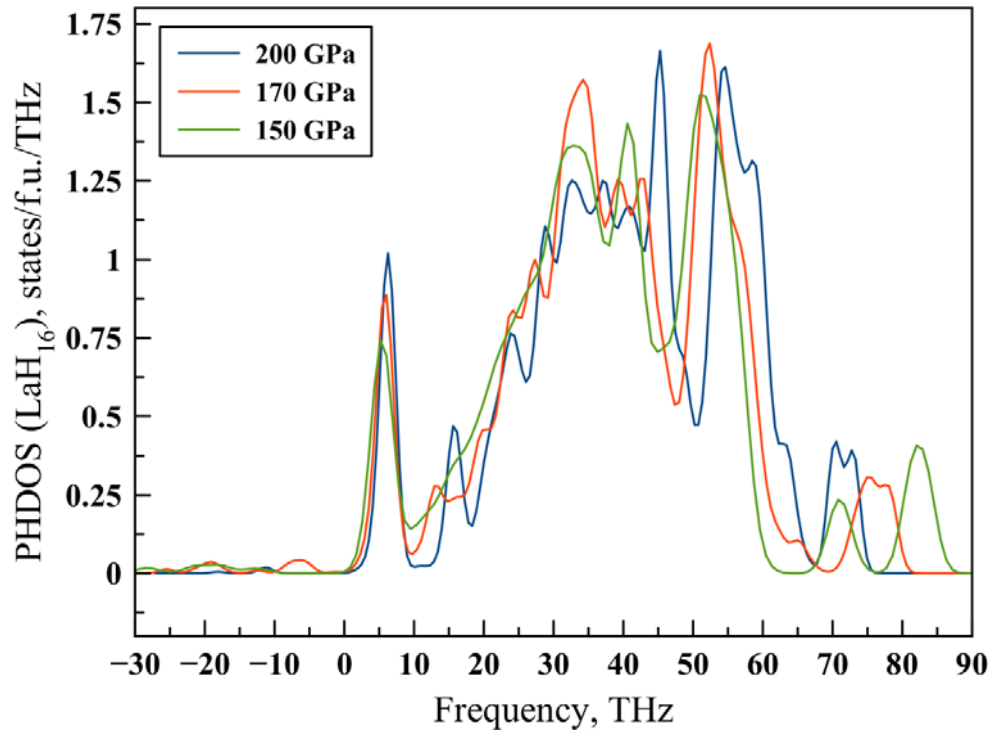


Fig. S5. Phonon density of states (DOS) of $P6/mmm$ -LaH₁₆ phase at 150, 170 and 200 GPa.

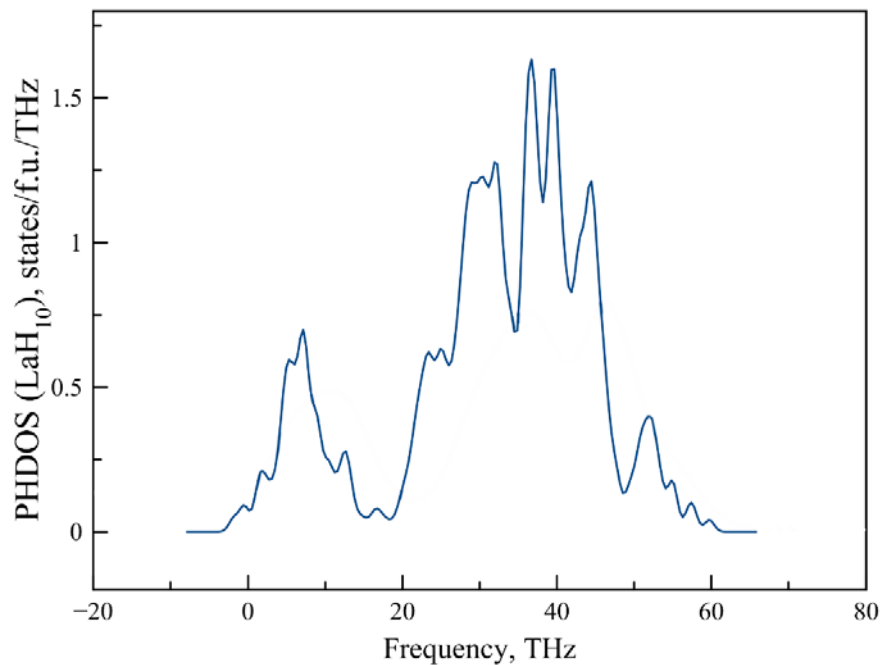


Fig. S6. Phonon density of states (smoothed) of $Fm\bar{3}m$ -LaH₁₀ at 150 GPa.

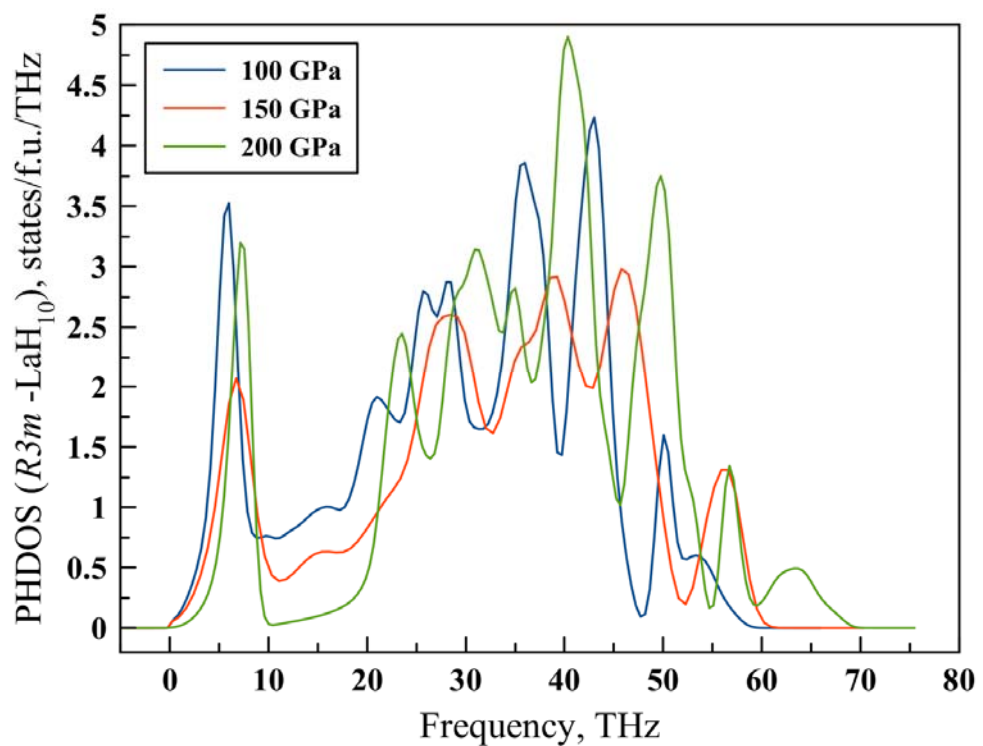


Fig. S7. Phonon density of states (smoothed) of $R\bar{3}m$ -LaH₁₀ at 100, 150 and 200 GPa.

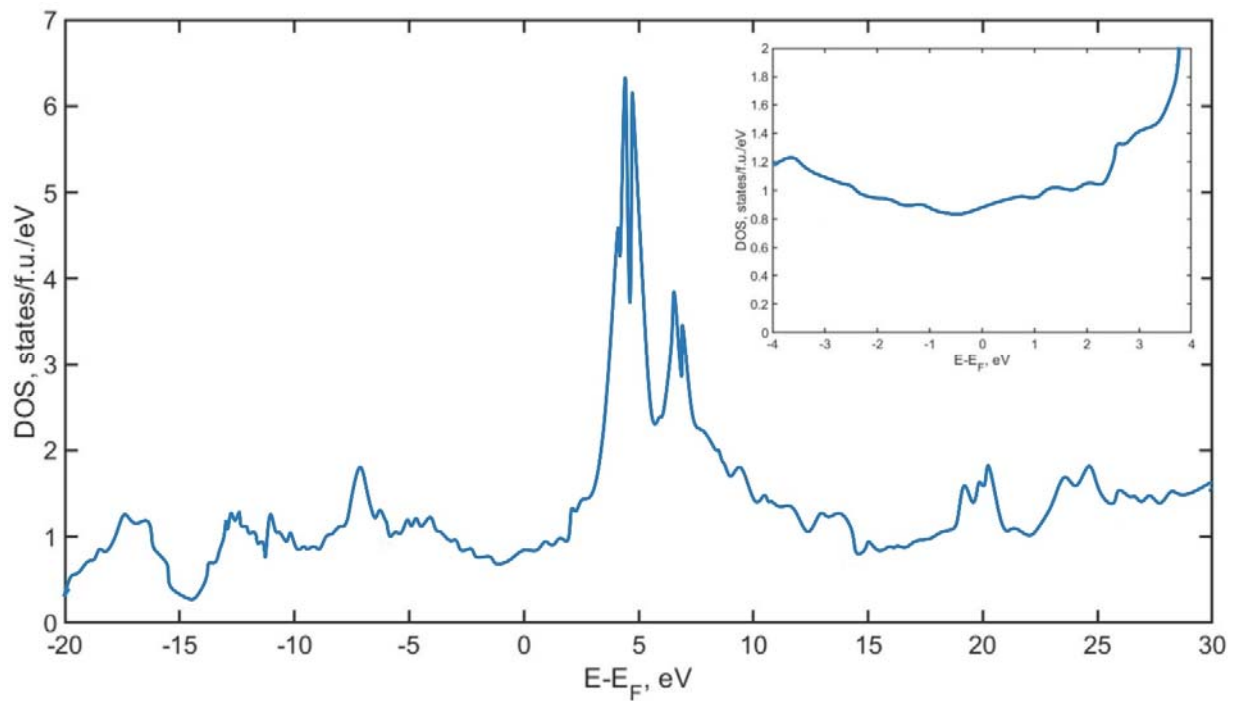


Fig. S8. Electronic density of states of $Fm\bar{3}m$ -LaH₁₀ at 200 GPa.

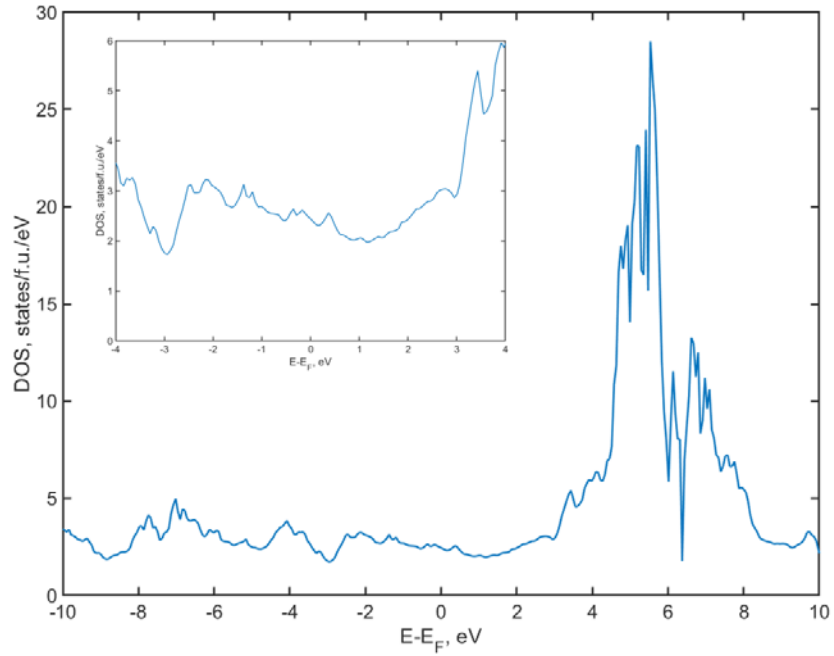


Fig. S9. Electronic density of states of $R\bar{3}m$ -LaH₁₀ at 165 GPa.

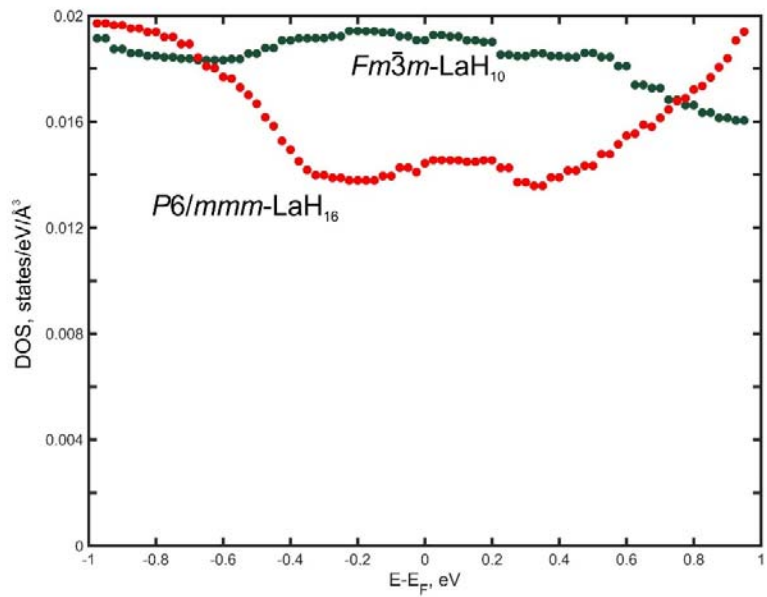


Fig. S10. Electronic density of states around the Fermi level in $Fm\bar{3}m$ -LaH₁₀ and $P6/mmm$ -LaH₁₆ at 200 GPa.

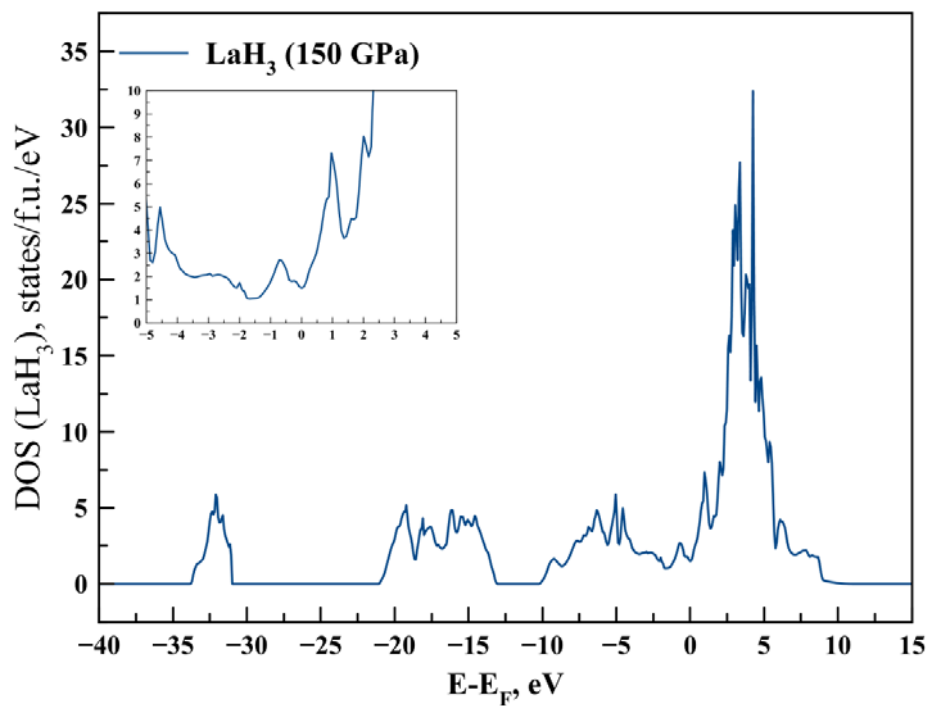


Fig. S11. Electronic density of states of $Cmcm$ -LaH₃ at 150 GPa.

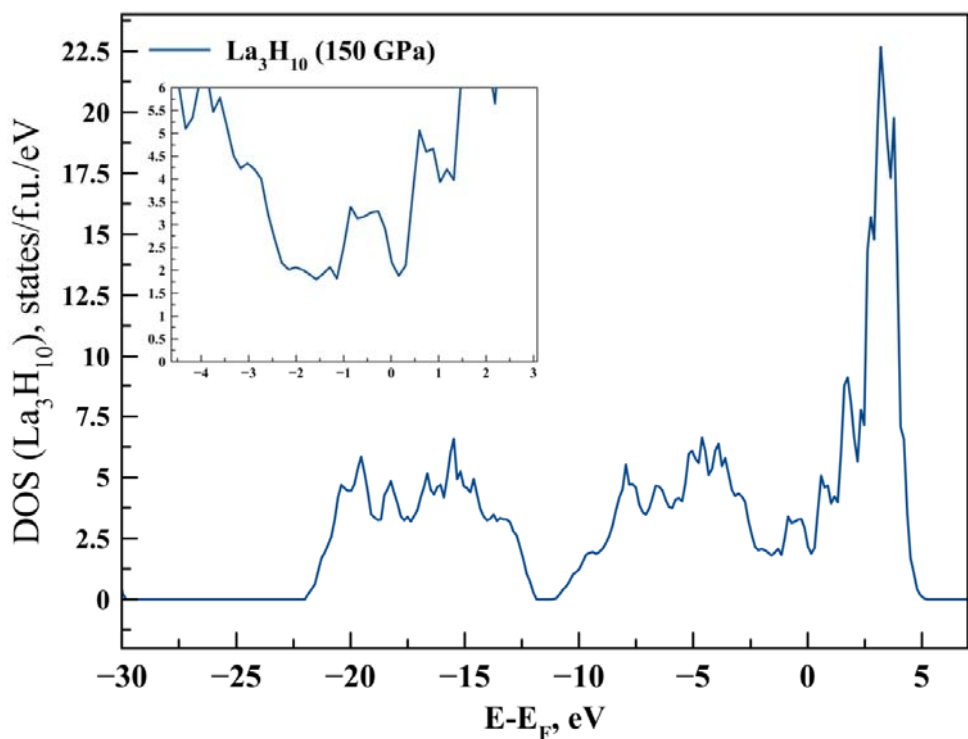


Fig. S12. Electronic density of states of *Cmmm*-La₃H₁₀ at 150 GPa.

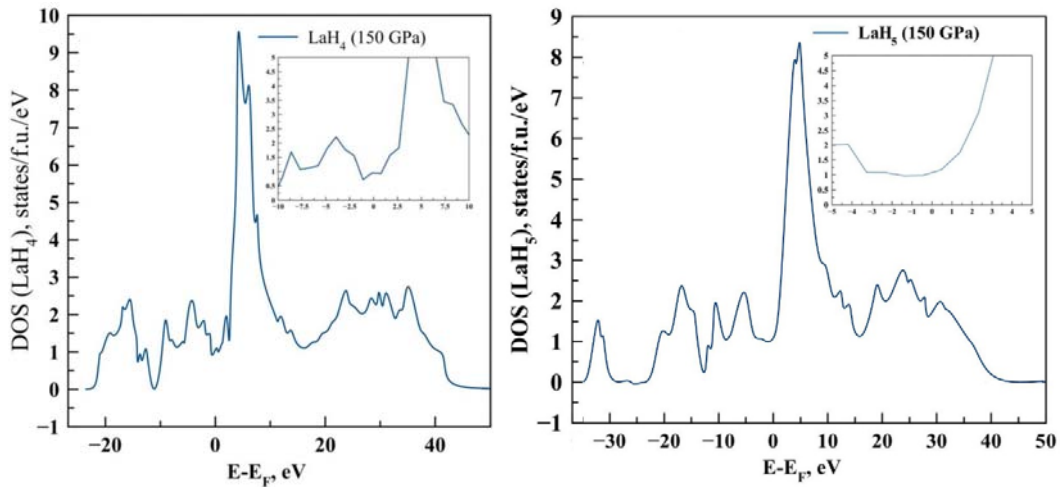


Fig. S13. Electronic density of states of *I4/mmm*-LaH₄ and *P* $\bar{1}$ -LaH₅ at 150 GPa.

Eliashberg spectral functions

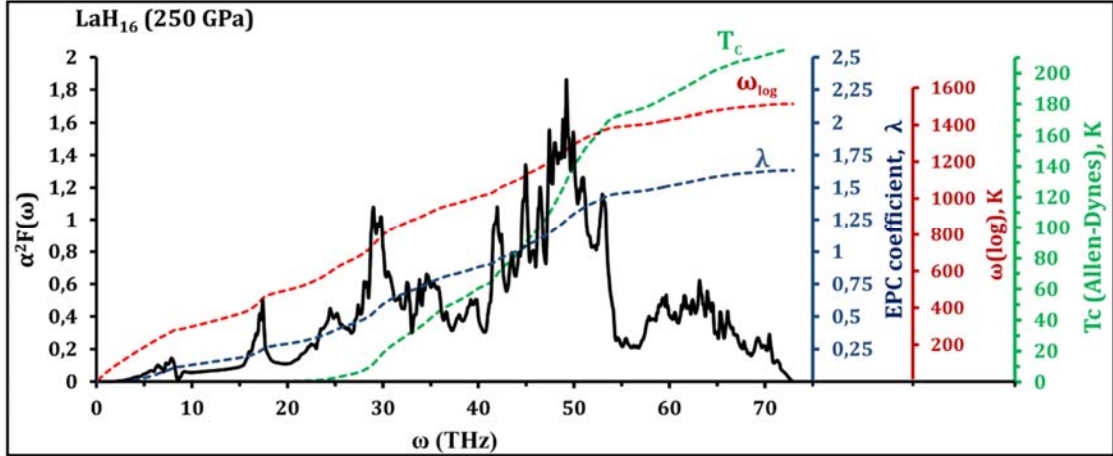


Fig. S14. Eliashberg function $\alpha^2 F(\omega)$ (black), ω_{\log} (red), EPC coefficient λ (blue), critical transition temperature T_c (green) of $P6/mmm$ - LaH_{16} at 250 GPa.

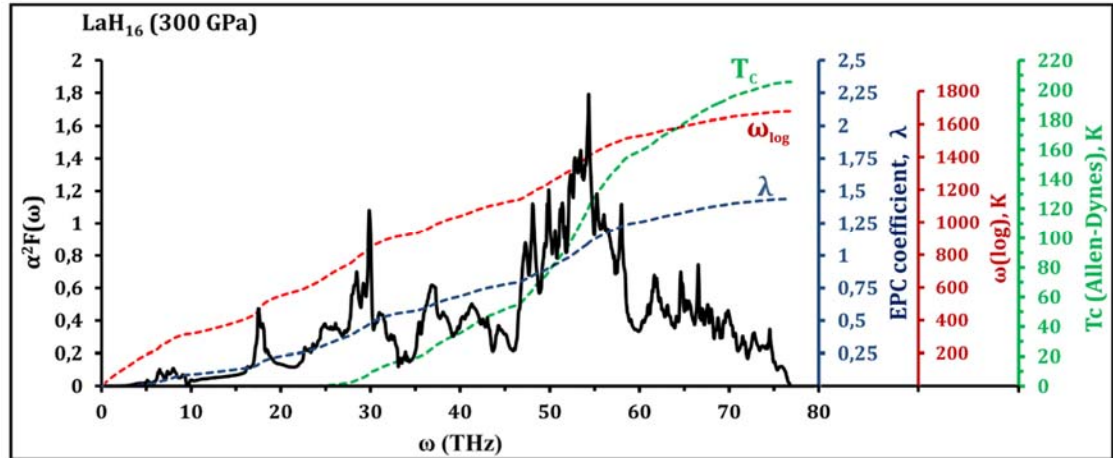


Fig. S15. Eliashberg function $\alpha^2 F(\omega)$ (black), ω_{\log} (red), EPC coefficient λ (blue), critical transition temperature T_c (green) of $P6/mmm$ - LaH_{16} at 300 GPa.

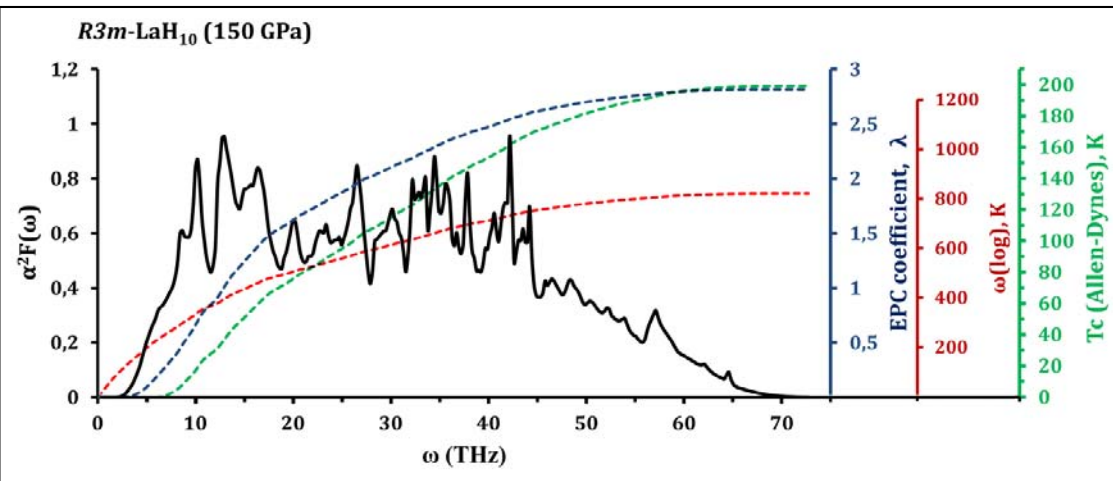


Fig. S16. Eliashberg function $\alpha^2 F(\omega)$ (black), ω_{\log} (red), EPC coefficient λ (blue), critical transition temperature T_c (green) of $R\bar{3}m$ - LaH_{10} at 150 GPa.

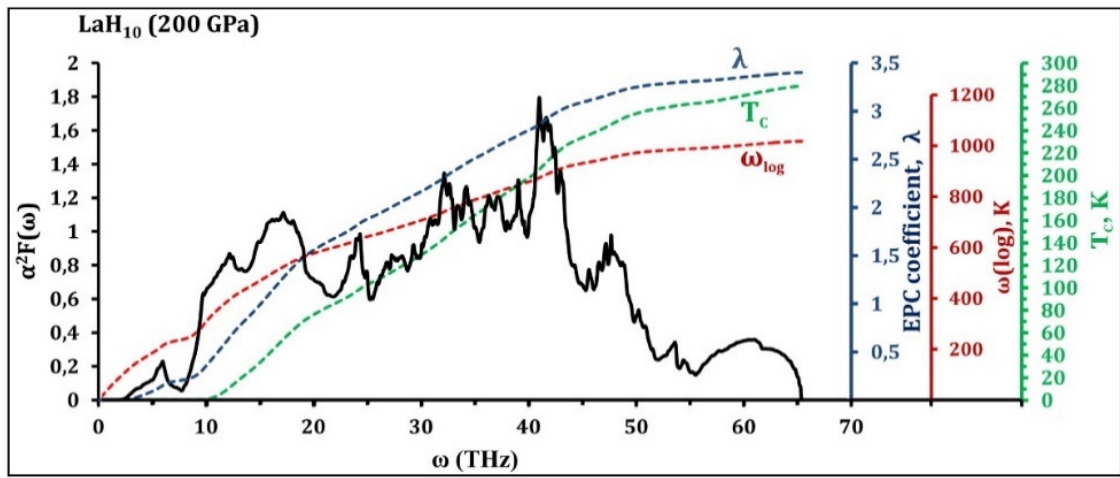


Fig. S17. Eliashberg $\alpha^2 F(\omega)$ function (black curve), and cumulative ω_{\log} (red), EPC coefficient λ (blue), critical transition temperature T_C (green) of $Fm\bar{3}m$ -LaH₁₀ at 200 GPa.

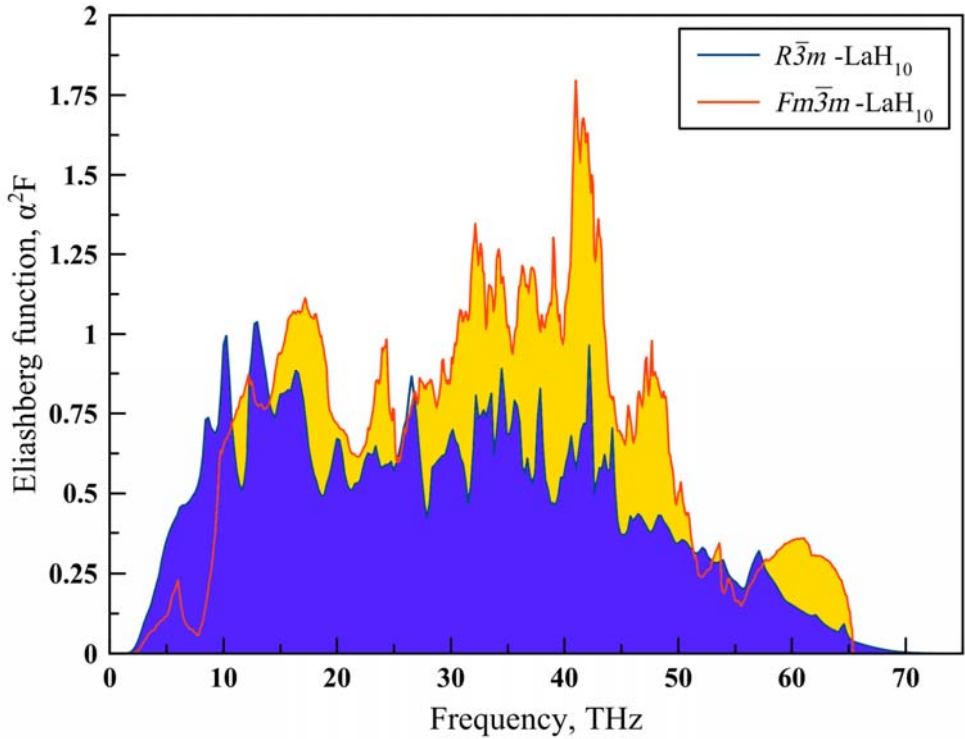


Fig. S18. Eliashberg functions $\alpha^2 F(\omega)$ of $R\bar{3}m$ -LaH₁₀ at 150 GPa (blue) and $Fm\bar{3}m$ -LaH₁₀ at 200 GPa (yellow).

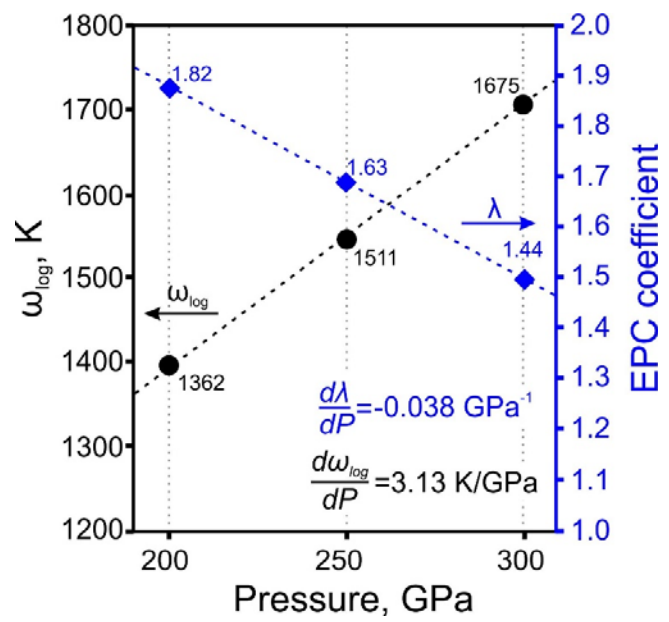


Fig. S19. Dependence of EPC coefficient and ω_{\log} on pressure for LaH₁₆.

Stability of LaH_{10} polymorphs

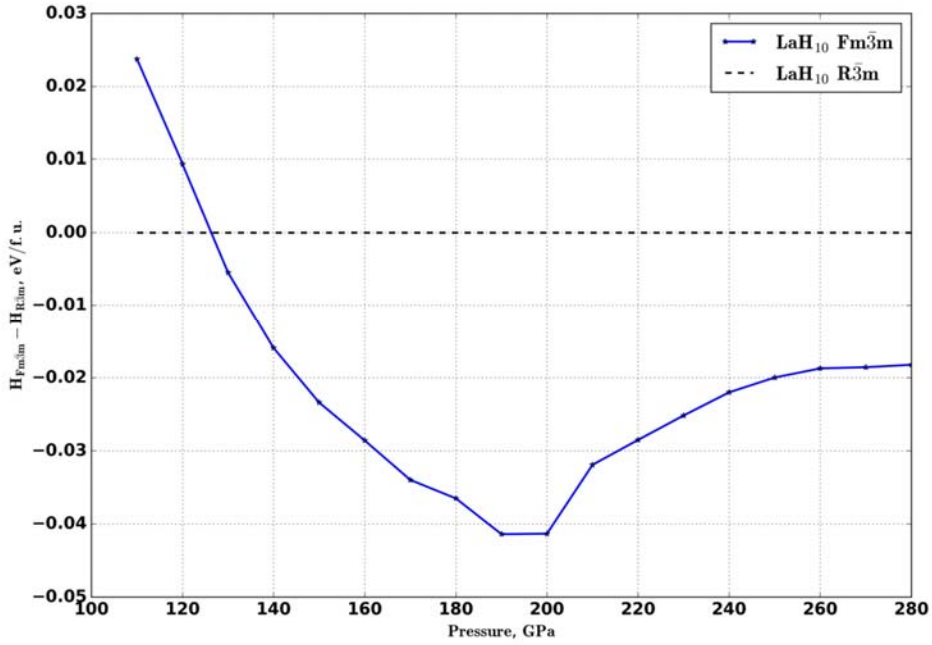


Fig. S20. Enthalpy difference between $Fm\bar{3}m$ - LaH_{10} and $R\bar{3}m$ - LaH_{10} . Undoubtedly, the transition $Fm\bar{3}m \rightarrow R\bar{3}m$ plays an important role in the measured record superconductivity of LaH_{10} . Such structural transitions accompany superconductivity in H_3S ($C2/c \rightarrow R\bar{3}m \rightarrow Im\bar{3}m$) [24], in Nb_3Al , V_3Ga [25] and in other well-known superconductors.

References

- [1] M. Lüders, M. A. L. Marques, N. N. Lathiotakis, A. Floris, G. Profeta, L. Fast, A. Continenza, S. Massidda, and E. K. U. Gross, Phys. Rev. B **72**, 024545 (2005).
- [2] M. A. L. Marques, M. Lüders, N. N. Lathiotakis, G. Profeta, A. Floris, L. Fast, A. Continenza, E. K. U. Gross, and S. Massidda, Phys. Rev. B **72**, 024546 (2005).
- [3] R. Akashi and R. Arita, Phys. Rev. B **88**, 014514 (2013).
- [4] R. Akashi, M. Kawamura, S. Tsuneyuki, Y. Nomura, and R. Arita, Phys. Rev. B **91**, 224513 (2015).
- [5] D. Pines, *Elementary Excitations in Solids : Lectures on Phonons, Electrons, and Plasmons* (Perseus, Reading, Mass, 1999).
- [6] J. Rath and A. J. Freeman, Phys. Rev. B **11**, 2109 (1975).
- [7] P. E. Blöchl, Phys. Rev. B **50**, 17953 (1994).
- [8] G. M. Eliashberg, JETP **11**, 696 (1959).
- [9] G. Bergmann and D. Rainer, Z. Für Phys. **263**, 59 (1973).
- [10] P. B. Allen and R. C. Dynes, Tech. Rep. 7 TCM41974 (1974).
- [11] R. Szczęśniak, Acta Phys. Pol. A **109**, 179 (2006).
- [12] R. Szczęśniak, Solid State Commun. **138**, 347 (2006).
- [13] A. P. Durajski, D. Szczęśniak, and R. Szczęśniak, Solid State Commun. **200**, 17 (2014).
- [14] K. S. D. Beach, R. J. Gooding, and F. Marsiglio, Phys. Rev. B **61**, 5147 (2000).
- [15] J. Bardeen, L. N. Cooper, and J. R. Schrieffer, Phys. Rev. **108**, 1175 (1957).
- [16] J. P. Carbotte, Rev. Mod. Phys. **62**, 1027 (1990).
- [17] A. P. Drozdov, M. I. Eremets, I. A. Troyan, V. Ksenofontov, and S. I. Shylin, Nature **525**, 73 (2015).
- [18] A. P. Drozdov, P. P. Kong, V. S. Minkov, S. P. Besedin, M. A. Kuzovnikov, S. Mozaffari, L. Balicas, F. Balakirev, D. Graf, V. B. Prakapenka, E. Greenberg, D. A. Knyazev, M. Tkacz, and M. I. Eremets, ArXiv181201561 Cond-Mat (2018).
- [19] P. B. Allen and R. C. Dynes, Phys. Rev. B **12**, 905 (1975).
- [20] H. Liu, I. I. Naumov, R. Hoffmann, N. W. Ashcroft, and R. J. Hemley, Proc. Natl. Acad. Sci. **114**, 6990 (2017).
- [21] N. P. Salke, M. M. D. Esfahani, Y. Zhang, I. A. Kruglov, J. Zhou, Y. Wang, E. Greenberg, V. B. Prakapenka, A. R. Oganov, and J.-F. Lin, ArXiv:1805.02060 <https://arxiv.org/ftp/arxiv/papers/1805/1805.02060.pdf> (2018).
- [22] I. A. Kruglov, A. G. Kvashnin, A. F. Goncharov, A. R. Oganov, S. S. Lobanov, N. Holtgrewe, Sh. Jiang, V. B. Prakapenka, E. Greenberg, and A. V. Yanilkin, Sci Adv **4**, eaat9776 (2018).
- [23] D. V. Semenok, I. A. Kruglov, A. G. Kvashnin, and A. R. Oganov, ArXiv180600865 Cond-Mat (2018).
- [24] I. Kruglov, R. Akashi, S. Yoshikawa, A. R. Oganov, and M. M. D. Esfahani, Phys. Rev. B **96**, 220101 (2017).
- [25] R. Viswanathan, Mater. Res. Bull. **9**, 277 (1974).